Final Technical Report

for

(ONR Grant No. N00014-93-1-0185)

CHEMICAL MECHANISTIC APPROACHES FOR THE SUPPRESSION OF SOOT FORMATION IN THE COMBUSTION OF HIGH ENERGY DENSITY FUELS

Prepared by

R. J. Santoro
Department of Mechanical Engineering
The Pennsylvania State University
University Park, PA 16802

Submitted to

Office of Naval Research
Propulsion and Energetics Program
Arlington, VA 22217

September 1996

DISCLAIMER NOTICE

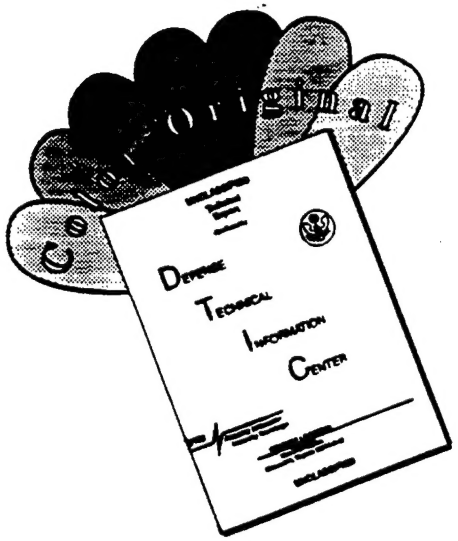

THIS DOCUMENT IS BEST QUALITY AVAILABLE. THE COPY FURNISHED TO DTIC CONTAINED A SIGNIFICANT NUMBER OF COLOR PAGES WHICH DO NOT REPRODUCE LEGIBLY ON BLACK AND WHITE MICROFICHE.

DISCLAIMER NOTICE

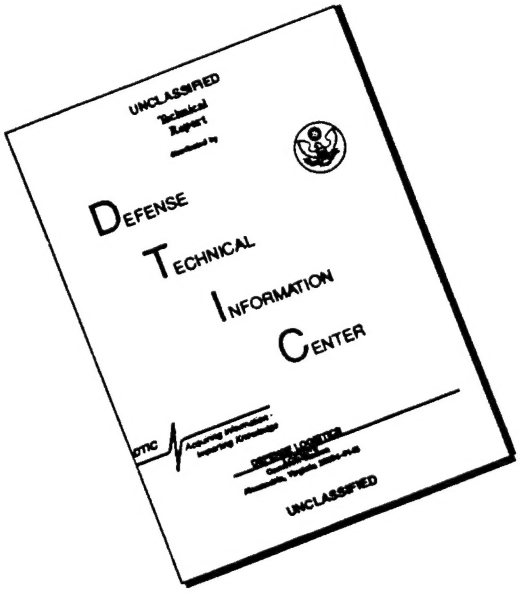

THIS DOCUMENT IS BEST QUALITY AVAILABLE. THE COPY FURNISHED TO DTIC CONTAINED A SIGNIFICANT NUMBER OF PAGES WHICH DO NOT REPRODUCE LEGIBLY.

Table of Contents

0.0 Abstract

Significant advantages can be gained by the use of high energy density fuels in volume limited applications. However, excessive soot formation that accompanies the combustion of these fuels presently limits their application. Fuel additive approaches prove attractive as they require minimal modifications to already existing equipment. In the present study, a variety of flame configurations were used to study the additive effects on soot formation. Through tests conducted on laminar diffusion flames carbon disulfide (CS_2) and methanol (CH_3OH) were found to be the most effective soot suppressants. Chemical interaction by either additive was found to far surpass the physical influences. However, the exact nature of the chemical action could not be established with the current set of experiments. Additionally, both of these additives were found to reduce soot formation in at least one high energy density fuel - quadricyclane (C_7H_8). To further validate this approach, studies were conducted using droplet flames and high-pressure spray flames.

1.0 Introduction

The interest in the development of compact, high-specific impulse propulsion devices has stimulated extensive research in the synthesis and use of high energy density fuels (HEDF). These fuels have a highly strained molecular structure (strain energies of the order 70 - 160 kcal/mole), which result in high heat releases on their combustion. Though, the strain energies are relatively small compared to the overall heat of combustion, they may result in significantly different combustion properties. Normal fuels, which are composed of stable molecules, require significant energy input to break the chemical bonds before the large energy release from combustion occurs. For strained molecules, it may be possible to release the energy stored in molecular strain at an early stage of combustion. This early energy release can enhance vaporization of these fuels and subsequent pyrolysis. Also, single droplet studies using solutions and slurries of these fuels show that reactions are not only limited to the gas phase. The liquid phase reactions of these fuels not only reduce the latent heat of vaporization, but also induce the droplets to micro-explode when they are internally heated to the limit of superheat [1].

Also, as seen in *Table 1,* values of heat release per unit (liquid) volume of these fuels are in excess (≥25%) of those typical to petroleum distillates. Such high values can mainly be attributed to the high density of these fuels. In fact, these fuels are quite often referred to as "high energy, high density fuels" in the literature. Such characteristics have implications towards longer flight range and decreased fuel tank sizes, and render the use of these fuels in volume-limited applications such as aircraft and rockets very attractive.

However, the present synthesis processes have not yet been perfected to an extent that these fuels can be obtained in sufficiently large quantities. Moreover, most of the synthesized fuels are solids at room temperature which precludes their use in the form of a spray. Initial efforts to use these fuels in the form of a solution were limited by their low solubility. Moriarty and Rao [2] have identified four potential high-energy-density fuels: (I) cubanes C_8H_8, (II) tetrahedrane C_4H_4, (III) quadricyclane C_7H_8, and (IV) dihydro benzvalene C_6H_6. While, I and II are not yet available by a feasible synthetic process. Both III and IV are liquids at room temperatures, a feature highly desirable for aviation

purposes. However, IV is limited by its proclivity to rearrange to isomeric benzene. Quadricyclane, on the other hand, is stable and is readily available commercially.

Heavy soot emissions, a characteristic common to the combustion of all of these fuels, serves as the chief limiting factor for their use in practical combustion devices. Studies on soot control among these fuels were limited by the inability to produce them in large quantities. Despite such limitations, a few studies have been performed investigating soot control amongst these fuels but with limited success. Law and Moriarty [3] observed the burning rate of these fuels could be enhanced by the addition of an azide group to the fuel molecules. The unstable azide group initiates the exothermic reaction

$$R\text{-}N_3 \rightarrow R\text{-}N + N_2, \qquad (1)$$

which leads to micro-explosion of droplets thereby enhancing the fuel vaporization and mixing. Similarly, modification of synthesis processes to add oxidative OH· radical to the fuel molecular structure seems possible at least in the case of benzvalene.

Table 1. Combustion characteristics of some typical high energy density fuels

Fuel		*Density (g/cm^3)*	*ΔH_R (kcal / g)*	*ΔH_R (kcal/liq. cm^3)*	*Strain Energy (kcal / g)*	*Remarks*
Petroleum Distillate	RP-1 ($C_8H_{15.54}$)	0.773	10.72	8.29	-	
High Energy Density Fuels	Cubane (C_8H_8)	1.29	10.90	14.06	1.548	solid
	Quadricyclane (C_7H_8)	0.982	10.87	10.67	0.854	
	Benzvalene (C_6H_6)	0.879*	10.65	9.36*	1.042	unstable
	Dihydrobenzvalene (C_6H_8)	0.710*	10.66	7.57*	0.908	difficult to process
Aromatics	Benzene (C_6H_6)	0.874	9.711	8.48	-	-
	Toluene ($C_6H_5CH_3$)	0.865	9.686	8.38	-	-

* These values are not well established, and are suspect for accuracy

2.0 Research Objectives

The motivation for the present research stems from the need to achieve soot control with the intended use of high energy density fuels for aviation purposes. Many previous investigations on jet engine emissions have reached the conclusion that design

modifications are the best method of achieving lower emissions. But design modifications may not be possible in all cases, particularly where the use of already existing hardware is intended. Considerations such as power and reliability at all operating altitudes sometimes make other solutions more desirable. Additionally, staged combustion systems, now prominently considered for NO_x reduction, also increase the tendency for sooting : a fuel rich primary zone is likely to enhance soot production. Thus even the best possible design modifications may still need help in the form of fuel modifications, or fuel additives to keep soot formation within acceptable levels.

With the above implications in mind, the following objectives have been identified for the present study :

1) Experimentally identify chemical additives which are effective in curtailing soot formation; attention being given to those which are liquids at room temperature and those that are easily blendable with fuels. Additionally, factors such as, toxicity and deposits, need to be considered which limit the present study to non-metallic additives.
2) Gain valuable insights into the chemical mechanisms active with the addition of these soot suppressants, and establish links, if any, to the already existing chemical kinetics database.
3) Based on the information gained, it is intended to make recommendations regarding potential molecular groups which may be directly incorporated into the molecular structure of these high energy density fuels during their synthesis process, so as to curtail soot formation.

3.0 Research Accomplishments

3.1 Experimental Methodology

Fuel additive approaches have long been employed for the control of soot emissions [4, 5]. A brief review of the literature reveals numerous additive influences to be effective that include both physical and chemical effects.

The physical influences are : temperature effects due to increased heat capacity of the additive; dilution by either inerts or by low sooting fuel additives; differential diffusion which reduces the concentration of soot precursor species; and reduced thermal diffusivities which result in smaller residence times in the soot growth region. The chemical influences are specific to the additive employed, and are usually associated with the changes induced in the radical concentrations important to the soot precursor formation.

It needs to be mentioned that most of the above influences are interdependent, and the above classification merely provides a basis for the discussion of each effect. A potential experimental methodology, besides evaluating the importance of each of these influences, should additionally identify the effects on various stages of soot formation - fuel pyrolysis, inception, surface growth and oxidation. The recent advances in this direction use integrated soot volume fraction [6], If_v, and critical strain rate, K_p [7], parameters which are too global to address processes occurring at the molecular level. For

the present purposes, an approach using co-annular laminar diffusion flames was followed, which allows examining the individual stages of soot formation.

As established by previous studies, co-annular flames with similar carbon atom flow rates have almost similar flame lengths [8]. Moreover, based on theoretical treatments by Kent and co-workers [9], the axial height can be normalised as $\eta = H/L_{cal}$ using a flame length calculated as [10]

$$L_{cal} = 1.330 \frac{Q_F}{\left(1+\frac{1}{S}\right)}, \tag{2}$$

where, L_{cal} is in mm, Q_F is the fuel flow rate in cm^3/s, and S is the stoichiometric molar air to fuel ratio. Similarly, the radial positions can be normalised as

$$\xi = r\frac{d_{f,eth}}{d_f}, \tag{2}$$

where, $d_{f,eth}$ is the diameter of a reference flame with ethene flow rate 3.85 cm^3/s, and it is assumed that the flame diameter scales as $d_f \propto (Q_F S)^{0.25}$. Further, it should be noted that the above normalization results in axial heights η being non-dimensional while the radial positions ξ have the dimensions of millimeters. Such a normalization enables the comparison of the measured scalar profiles among different flames. This aspect proves instrumental for the present purposes where flames of different fuel compositions are studied.

3.2 Experimental Techniques

Table 2. lists the techniques employed to measure the scalar properties relevant to this study. Though these techniques are briefly discussed below, the reader is referred to the corresponding references for further details.

Table 2 : Measurement techniques employed in the present study.

Parameter Measured*	**Technique Employed**	**Reference**
f_v	Laser Induced Incandescence (LII)	[11,12]
D_{63}, N	LII & Laser Light Scattering (LLS)	[13]
T (Kelvin)	Rapid insertion thermocouple technique	[14]
[OH^-], [OD^-]	Fluorescence	[15]
[Small PAH], [Large PAH]	Fluorescence	[16]
[Stable Species]	Gas-Chromatography	[17]

* [...] represents concentration of the respective species

3.2.1 The Burner and Vaporizer System :

A schematic of a co-annular laminar diffusion flame arrangement is shown in Fig. 1. In this flame gaseous or a prevaporized fuel is passed from a central fuel tube while air passes through the outer concentric tube. The flow conditions prevailing at the exit of the tubes ensure a laminar flow. A flame is established in the mixing region of these flows, where close to stoichiometric conditions are established. In such an arrangement, the various stages involved in soot formation, i.e., inception through oxidation, are spatially separated, which allows one to examine the effects of various operating conditions on each of these processes. As overventilated versions of these flames are highly reproducible and stable, an abundance of literature has been established in this configuration.

For reasons mentioned above, co-annular laminar diffusion flames were used in this study. Furthermore, the data and understanding that has already been established in our laboratory was expected to be instrumental. Fig. 1. shows a schematic diagram of the burner used in this investigation. It consists of a 1.11 cm internal diameter brass fuel tube within a concentric 10.2 cm internal diameter brass air annulus. The fuel tube extends 0.4 cm above the air annulus which is 12.5 cm long. The air annulus contains a series of gage-70 wire meshes, a 0.3 cm glass bead bed and, finally a 2.54 cm thick ceramic honeycomb (Corning-0.15 cm cell size) which provide flow conditions to achieve a uniform flow at the exit of the burner. A 46 cm long brass chimney shields the flame from laboratory air currents. Slots machined in this chimney besides providing optical access, were also used to introduce sampling probes and thermocouples.

The vaporizer consisted of a swagelok "Tee" section stuffed with glass wool. The temperature of this "Tee" section along with that of the burner was monitored by electric heaters wrapped around this system. Liquid additive was introduced into the fuel stream using a syringe pump. Sufficiently stable flames could be achieved in this system even while having no flow through the carrier fuel stream.

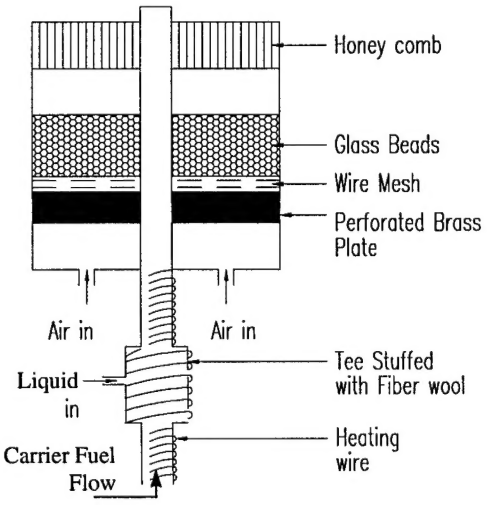

Figure 1. Co-annular laminar diffusion flame burner and the vaporizer system used to introduce liquid additives

3.2.2 Soot Aerosol Characterization :

Laser-induced incandescence (LII), a recently perfected technique, was used in measuring the soot volume fraction in various flames. In this technique, laser radiation is used to heat soot particles close to their boiling point (i.e., about 3700 K), and the ensuing radiant emission from these particles when collected after an appropriate time interval and in a certain spectral band is found to be proportional to the local soot volume fraction. Fig. 2. shows a typical experimental setup to measure 2-D LII. A 285 mJ/pulse, near-Gaussian-profile beam from the YAG laser was shaped into a 350 μm thick (FWHM) laser sheet with a combination of a diverging cylindrical lens (focal length = 6 cm) and a spherical lens (focal length = 2 m). An aperture placed in front of this lens combination allowed one to use only the central portion of the laser sheet, thereby providing a uniform laser sheet at the focal point.

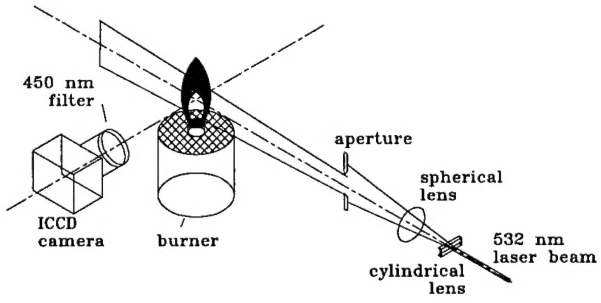

Figure 2 : A typical experimental setup to measure planar laser-induced incandescence

The LII images were collected by an image intensified CCD camera (Princeton Instruments, Model ICCD-576S/RB) placed perpendicular to the laser sheet. A combination of a 105 mm focal length UV lens (Nikon, f/4.5) and an interference filter (450±25 nm) placed in front of the camera helped in collection of the LII image. Interference from the scattered laser radiation was avoided by collection of the signal 20 ns following the laser pulse through the flame. The LII signal collection was limited to a time period of 18 ns, which is much shorter than the LII signal decay time (approx. 500 ns), to avoid signal variations due to differences in particle size.

In a similar setup, laser light scattering (LLS) measurements were performed by having a 532±2 nm interference filter in front of the camera and by limiting the signal collection to the advent of the incident laser pulse. Values of the volumetric cross-sections, Q_{vv}, were obtained by calibrating the signals from a pure ethene jet. Such measurements can be used with local soot volume fraction information to obtain soot particle size and number density information. Assuming the particles to be within the Rayleigh regime, i.e, $(\pi D/\lambda) \leq 0.3$, the mean particle diameters can be calculated as

$$D_{63} = \lambda^{4/3}\left(\frac{2Q_{vv}}{3\pi^3 F(m) f_v}\right)^{1/3}, \tag{3}$$

where, for the complex index of refraction m,

$$F(m) = \left|\frac{m^2 - 1}{m^2 + 2}\right|^2 . \tag{4}$$

Similarly, number densities can be evaluated as

$$N = \frac{12 f_v}{\pi D_{63}^3} . \tag{5}$$

3.2.3 Rapid Insertion Thermocouple Technique :

In moderately sooting flames ($f_v \approx 1$ - 20 ppm), temperature measurement by thermocouples is difficult due to interferences from soot deposited on the thermocouple beads. In such flames, a rapid insertion thermocouple technique, similar to the one used by Kent and Wagner [14], was employed. In this technique, soot deposited on the thermocouple is burnt away by placing it in an oxygen rich region of the flame where temperatures in excess of 1500°C are achieved. Such "burn-off points" in the flame are predetermined through a few trial measurements. At any measurement point, shorter residence time for the thermocouple is recommended to avoid soot deposition effects. However, sufficient time needs to be allowed for the thermocouple to be in equilibrium with its surroundings. A computer controlled stepper motor system and a data acquisition system were instrumental in performing such measurements.

To minimize interference effects, fine wire thermocouples - with bead diameters in the range 150 - 250 μm - were used. Also, a forked prong arrangement as used previously by Richardson [18] minimizes effects due to conduction, as well as, those due to interference. The measured temperatures were corrected for radiation losses.

It needs to be mentioned that in heavily sooting flames (f_v > 20 ppm), soot deposition effects are aggravated to an extent that accurate temperature measurements are not possible. Also, in these heavily sooting flames, energy dissipation through radiative processes is very high, and the consequent temperatures are so low that "burn off" of soot cannot be achieved.

3.2.4 Laser Induced Fluorescence - $OH^{\cdot}$, $OD^{\cdot}$:

Hydroxyl radical (OH) has long been identified to be one of the important oxidative species during combustion. Also, regions of high $OH^{\cdot}$ concentration are believed to represent regions of high chemical activity thereby identifying the flame front.

The experimental arrangement (*cf.* Fig. 3.) for OH radical fluorescence is similar to the one followed by Puri et. al. [15]. The output from a YAG pumped dye laser after frequency doubling is focused at the center of a laminar diffusion flame. The dye laser was tuned to a wavelength of 283.55 nm which corresponds to the $Q_1(8)$ line of the $A^2\Sigma^+ \leftarrow X^2\pi_i$ (1,0) band of $OH^{\cdot}$. Excitation from the N"= 8 level was selected in order to minimize the Boltzmann population correction with temperature (less than 5% over the

range 1400 to 2100 K). Low laser energies were utilized to ensure that the fluorescence signals measured were within the linear regime. The signal was collected using a micro channel plate intensified CCD camera interfaced with a personal computer. WG320 and UG11 glass filters along with a UV Nikon lens used in front of the camera limited signal collection to a spectral band ranging between 270 - 320 nm (50 % transmission cut-off). This procedure allowed signal collection corresponding to the (0,0) and (1,1) emission bands of the OH, while avoiding the scattered laser light from the soot particles. Corrections due to the absorption of the incoming beam for the $Q_1(8)$ transition were expected to be small and were not incorporated. Furthermore, errors due to fluorescence trapping were expected to be minimal.

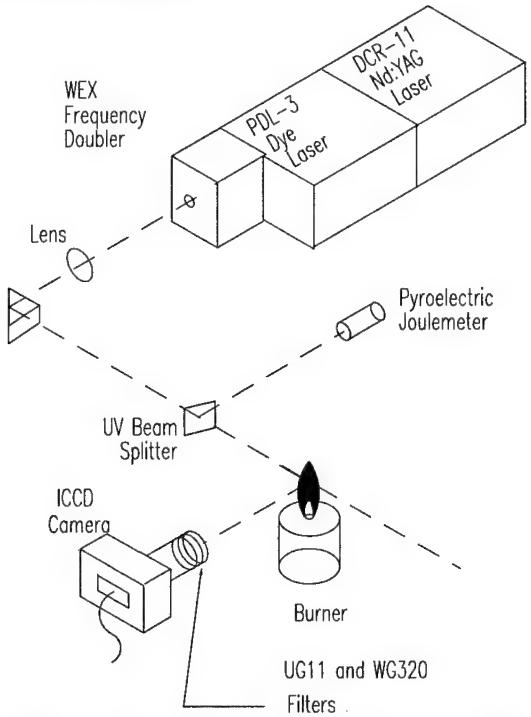

Figure 3. : Schematic of the experimental arrangement for OH, OD laser-induced fluorescence.

Interference from broad band PAH fluorescence and laser-induced incandescence signals can be minimized by noting that they are spatially well separated from the OH fluorescence signal. Also, as PAH fluorescence lifetime is much larger than OH fluorescence lifetime interference from PAH can be minimized by operating the camera with gate as small as possible (5-18 ns typical). Also, interference from laser-induced incandescence is avoided by using sufficiently small laser fluence levels.

Absolute concentrations were obtained by carrying over calibrations from the measurements of Puri et al. [15].The measured signals were corrected for quenching following a novel method. While using the quenching cross-sections suggested in reference [19], estimates of quenching for equilibrium mixtures at stoichiometries between 0.6 and 1.6 were obtained for the three flames of interest to this study - C_2H_4, C_2H_4 + 25% CH_3OH and C_2H_4 + 25% CS_2. Correction factors based on such estimates, C, allowed the transfer of calibrations from the pure ethene flame to the other two flames where different amounts of H_2O and CO_2 - species accounting for nearly 70% of

fluorescence quenching -are expected to be formed. Subsequently, absolute OH radical concentrations were obtained as

$$[OH^{\cdot}] = [OH^{\cdot}]_{ref} \left(\frac{S}{S_{ref}} \right) \sqrt{\frac{T_{ref}}{T}} \left(\frac{C}{C_{ref}} \right), \qquad (6)$$

where, S is the signal, and T the local temperature in degrees Kelvin. For the present measurements, the peak $OH^{\cdot}$ concentration values at 20 mm axial height in a 3.85 cc/sec ethene flame were used as reference values. At the flame temperatures the variation of the quenching rate upon the initially excited rotational level (N'= 8 and N'= 10 for the transitions studied here) is expected to be less than 10% [19].

In a similar manner, relative $OD^{\cdot}$ fluorescence signals were obtained with laser excitation at 287.680 nm.

3.2.5 Laser Induced Fluorescence - PAH :

As mentioned earlier, PAH constitute the aromatics from 1-ringed compounds like benzene to large multi-ringed compounds such as coronene. As it is difficult to devise an optical scheme to measure the concentrations of each of these species, it is only possible to measure the relative concentrations of small and large PAH molecules.

For excitation in the UV at 266 nm, the fluorescence spectrum from small PAH (≤2 aromatic rings) is as shown in Fig. 4. As observed these molecules, mainly constituting of acenapthalene, show a single peak at ~ 280 nm, while exhibiting very little fluorescence in the visible. For similar excitation, the fluorescence spectrum by large PAH molecules (2≤ number of aromatic rings ≤ 4), exhibits a bimodal nature with an additional peak in the visible (~ 480 nm). Based on such spectral differences, one can obtain estimates about the relative concentrations of either species by collecting fluorescence signals in the UV (~ 280 nm) and in the visible (~ 480 nm) wavelengths. It should be noted that our previous scheme [20] which was based on fluorescence spectra at room temperatures [21] differs considerably from the present one.

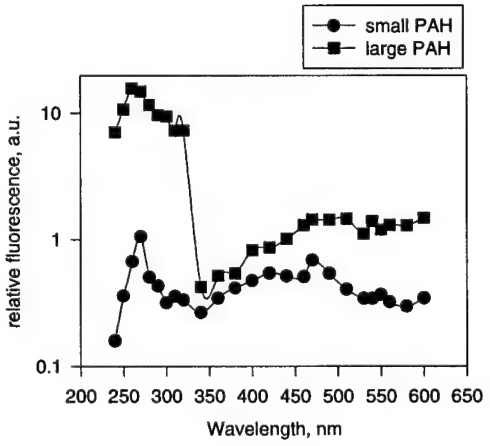

Figure 4. : The fluorescence spectra of small and large PAH species when excited by laser light at a wavelength of 266 nm.

The experimental arrangement used for these measurements was similar to the one used for OH fluorescence measurements (*cf.* Fig. 3.). The 532 nm output from a Nd:YAG was frequency doubled and the ensuing 266nm beam was focused at the center of flame. UV fluorescence signals were collected by using a combination of WG295 and UG11 Schott color glass filters, while the visible fluorescence was collected by using a 500±5 nm interference filter. To reduce interferences due to Rayleigh scattering the 266 nm beam was horizontally polarized. Additionally, the signal collection was delayed by 12 ns from the peak of the laser pulse. Also, very low laser fluences (≤ 50 μJ/pulse while using 1.0 m focal length lens) were used to ensure minimal interference from the C_2 fluorescence [16] and laser-induced incandescence.

3.2.6 Gas Chromatography :

The gaseous species at various points in the flame were sampled using an electro-mechanical-sonic probe [17]. They were further pressurized using a piston-cylinder arrangement and stored in a 16 loop Valco valve system for later analysis. A gas chromatograph equipped with Porapak Q and Porapak S columns in series with a molecular sieve, and using TCD and FID detectors, enables the determination of concentrations of species up to C_6H_6. However, by following such a procedure, the sum of the measured mole fractions would usually be less than unity (typically ~ 0.8), and a normalization was performed to establish concentrations on an absolute scale. Additionally, using the present setup, mole fractions of SO and SO_2 could not be determined in flames to which CS_2 was added. Equilibrium calculations for stoichiometries between 0.6 and 1.6 in C_2H_4 + 25%CS_2 flames, show SO and SO_2 concentrations to be less than 4%. Accordingly, little error should be introduced into the overall analysis by neglecting their concentrations. Also, it needs to be mentioned that the measured concentrations of stable species would have a contribution from the radicals in the gas sample. To illustrate this point further, the measured C_2H_4 concentrations would have contributions from radical recombinations, such as, C_2H_3 + H and CH_3 + CH_3 followed by dehydrogenation.

By using the above techniques, considerable effort was spent to identify potential additives for soot control. Amongst those tested, CS_2 and CH_3OH were found to be the most effective. Subsequently, further experiments were conducted to identify the mechanisms by which these additives influence soot formation.

3.3 Ethene Laminar Flame Studies

Ethene laminar diffusion flames were established with the carbon atom flow rate held constant, i.e., with a value equivalent to an ethene fuel flow rate of 3.85 cm^3/s (*cf.* Table 3.).

3.3.1 Variations in Soot Particle Field :

Planar images of soot volume fraction, f_v, number density, N, and mean particle size, D_{63}, were obtained using LII and LLS techniques. On comparing the f_v images of the flames of interest, one notices soot reductions up to 60% with methanol addition and up to 80% with CS_2 addition (*cf.* Fig. 5). Most notable features upon methanol addition are,

(a) the shorter flame length, and (b) the substantially diminished number densities. Similar features upon CS_2 addition are, (a) the reduction in the particle size (which is not the case upon methanol addition), and (b) the suppression of soot formation in the annular region.

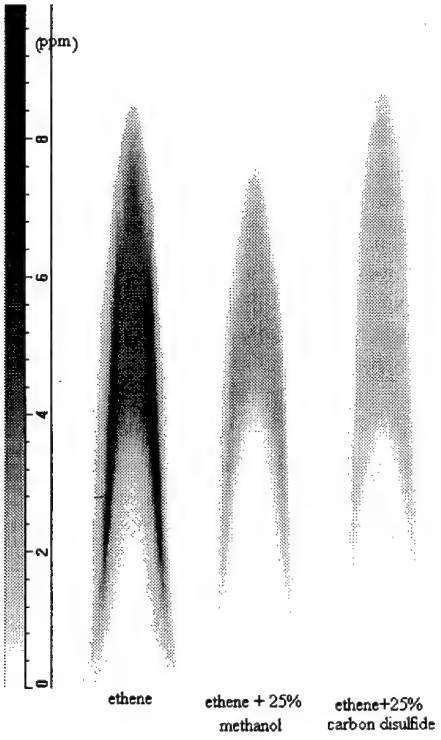

Figure 5. Planar images of soot volume fraction in C_2H_4, C_2H_4 + 25% CH_3OH, and C_2H_4 + 25% CS_2 flames.

Table 3. Flow rates for ethene flames

Fuel	cm^3/s	Additive	cm^3/s	Mole% of additive	C % of additive	T_{ad} (K)
C_2H_4	3.85					2370
C_2H_4	3.30	CH_3OH	1.10	25.0	14.2	2347
C_2H_4	3.30	CH_4	1.10	25.0	14.2	2345
C_2H_4	3.30	CS_2	1.10	25.0	14.2	2346
C_2H_4	3.30	CO_2	1.10	25.0	14.2	2328

**Air flow rate for all the flames is 1060 cc/sec

3.3.2 Temperature Effects :

The temperature effects introduced upon CH_3OH addition were determined by comparing with the temperature profiles in a C_2H_4 + 25% CH_4 flame. While the temperature profiles, at heights 7-20 mm, in both the flames are quite similar, appreciable soot reductions could be observed upon methanol addition. This could not be due to the extra soot formed upon CH_4 addition, because the amount of soot formed in CH_4 is only about one-twentieth of that formed in C_2H_4 [23]. Also, the temperatures in the methanol added flame are higher by ≈ 10-20 K. Such observations eliminate the possibility of soot reduction due to temperature changes and suggest alternate mechanisms to be active.

Similar evaluations by comparing the temperature profiles in C_2H_4 + 25% CS_2 and C_2H_4 + 25% CO_2 flames were inconclusive. However, the adiabatic temperatures of C_2H_4 and C_2H_4 + 25% CS_2 flames agree to within 24 K, whereupon one cannot account for the large soot reductions merely based on temperature effects. The use of adiabatic flame temperature as the characteristic flame temperature is well accepted, and is discussed at length by Gomez and Glassman [24], and Axelbaum and Law [25].

3.3.3 Dilution :

One possible way to evaluate dilution is to obtain measurements of f_v while varying the amount of the additive; a linear decreasing trend in $If_{v,max}$ with increasing mole fraction of the additive would be suggestive of a dilution effect [6]. Instead of performing such a procedure, we compared the ethene concentration profiles in these flames. Minimal variations in C_2H_4 concentrations upon CH_3OH and CS_2 addition (*cf.* Fig. 6) attribute minimal possibility of soot reduction due to dilution. Recently, Santoro and coworkers [26] have made similar observations. They attributed the reduced dilution effects to diffusional transport of N_2 from the surrounding air, which tends to establish almost similar fuel concentrations at short distances downstream of the fuel tube.

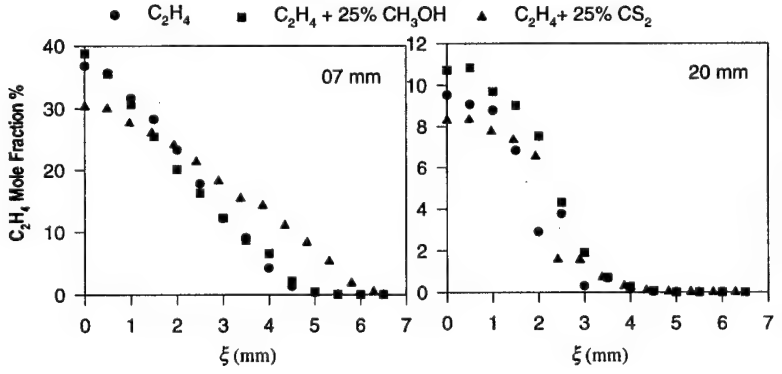

Figure 6. Ethene concentration profiles in ethene, ethene+25% methanol and ethene+25% CS_2 flames. The radial position ξ is normalized as in eqn. 2.

Also, the methanol pyrolysis and oxidation mechanism [27], suggests that almost 80% of it follows a non-sooting pathway, resulting in the formation of CO and finally CO_2. If this is the case, one should observe similar soot reductions upon addition of HCHO to C_2H_4; HCHO is an intermediate in the conversion of CH_3OH to CO. Contrary

to these expectations, HCHO addition was found to promote soot. This further ascribes negligible dilution effects towards the formation upon methanol addition.

3.3.4 Differential Diffusion :

Another physical process that needs consideration is differential diffusion. As both CH_3OH and CS_2 have diffusivities similar to that of C_2H_4, this effect is expected to be relatively small (*cf.* Table 4).

3.3.5 Thermal Diffusivity (Residence Time) Effects :

Values of thermal diffusivities, α, of various species at 1 atm and 1000 K are given in Table 4. Lower values of α would result in temperature profiles with steeper gradients. As soot inception is expected to have a threshold of 1350 K, inception and subsequent growth should be confined to a narrow annular region adjoining the flame front, thereby reducing the time available for surface growth [28]. Such an effect should be more pronounced upon CS_2 addition as it has a very low value of α. Contrary to this argument, the measured temperature profiles in C_2H_4 + 25% CS_2 do not show any appreciable gradients, thereby suggesting other mechanisms to be relatively dominant.

Table 4 : Binary diffusion coefficients in N_2, $D_{i/N2}$, and thermal diffusivities, α, at 1 atm and 1000 K

Species	α (cm^2/s)	$D_{i/N2}$ (cm^2/s)
C_2H_4	1.110	1.3522
CH_3OH	1.066	1.3590
CH_4	1.937	1.7960
CS_2	0.464	0.9436
CO_2	1.043	1.3133
H_2	11.64	6.0236

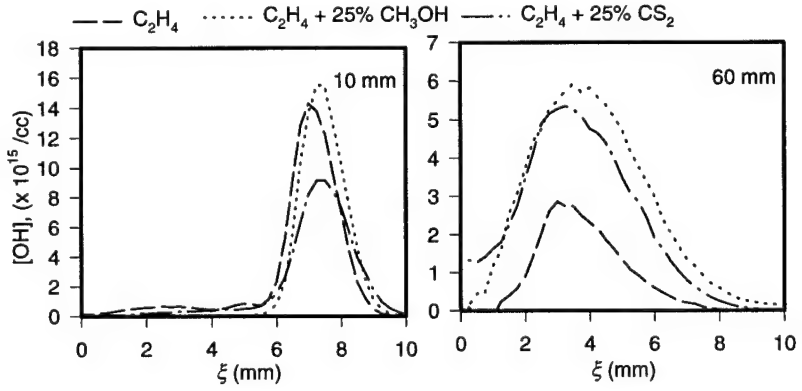

Figure 7. OH· fluorescence profiles in C_2H_4, C_2H_4 + 25% CH_3OH, and C_2H_4 + 25% CS_2 flames.

3.3.6 Chemical Effects :

As identified above, the strong soot suppressions accompanying the addition of CH_3OH and CS_2 appear largely to be a chemical effect. Further efforts were focused to identify potential chemical mechanisms leading to such soot reductions. The observed trends upon the addition of CH_3OH and CS_2 were different, and are discussed below separately.

CH_3OH addition :

Upon methanol addition, the OH· concentrations remain relatively unaltered at lower heights (*cf.* Fig. 7) in a region where PAH formation and soot inception are prominent. At higher locations methanol pyrolysis results in higher OH· concentrations. However, the chemical mechanism leading to enhanced OH· production from methanol is not very clear. As discussed by Westbrook and Dryer [27], the pyrolysis of methanol into CH_3 and OH radicals is less likely. In fact one makes an interesting observation by measuring OD· fluorescence upon CD_3OD and CH_3OD addition; the OD· concentrations in the former were exactly four times those in the latter. This suggests that all of the H atoms in CH_3OH have an equal probability of conversion to OH. However, due to the lack of supportive evidence it could not be confirmed whether such a conversion is limited to CH_3OH alone amongst all the alcohols.

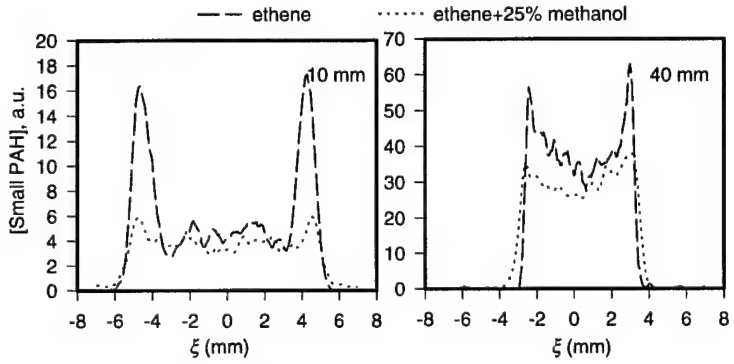

Figure 8. Fluorescence measurements of small PAH species in C_2H_4, and C_2H_4 + 25% CH_3OH flames.

The magnitude of the observed increases in OH· concentrations at higher flame locations is not significant enough to account for the large (60-80%) reductions in soot formation. Notwithstanding the above noticed increases in oxidation by OH·, it appears that soot formation processes prior to oxidation are significantly altered.

If we are to assume, fluorescence to be proportional to the local concentrations of these species, one observes some interesting trends. The formation of both small and large PAH appear to be greatly diminished (≈40%) upon methanol addition. Frenklach and Yuan [29] and Alexious and Williams [30], observed the formation and growth of PAH species to be strongly governed by the H radical concentrations, and they further attribute diminished PAH formation to lower values of H radical superequilibrium,

$$f = \frac{[H]^2/[H_2]}{[H]_{eq}^2/[H_2]_{eq}}. \tag{7}$$

The decrease in f was attributed to the excessive molecular hydrogen that was produced during methanol decomposition. However, in the present study, estimates of f could not be obtained due to experimental difficulties associated in measuring both [H·] and [H_2]. Such measurements are critical to fully understand soot suppression in these flames.

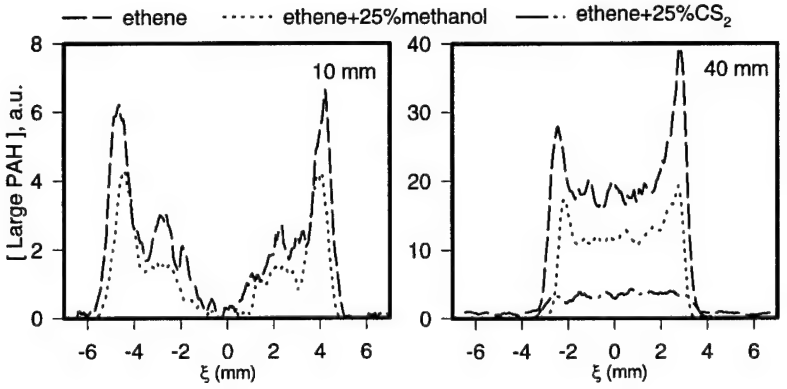

Figure 9. Fluorescence measurements of large PAH species in C_2H_4, C_2H_4 + 25% CH_3OH, and C_2H_4 + 25% CS_2 flames; note that the PAH concentrations in C_2H_4 + 25% CS_2 flame at 10 mm height are negligibly small.

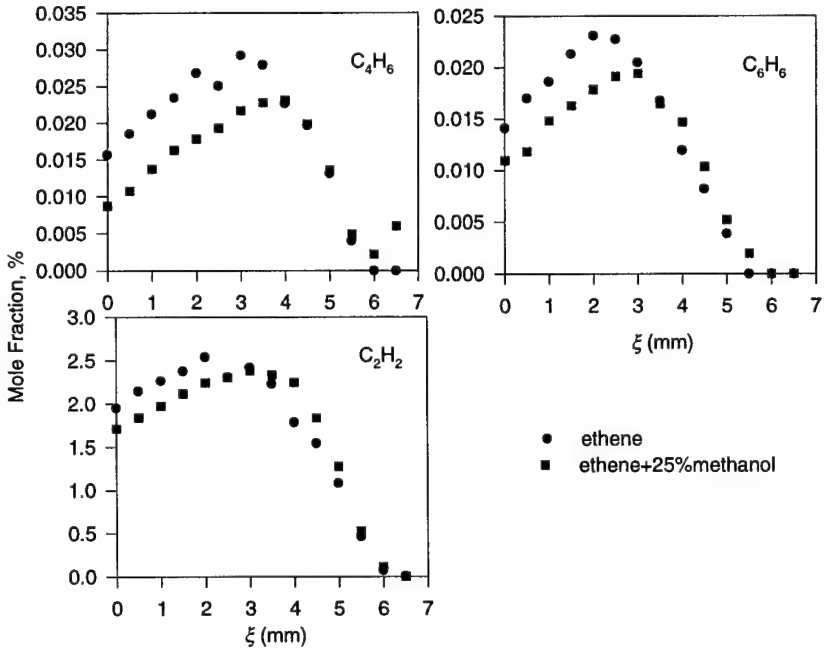

Figure 10. Stable species profiles in C_2H_4 and C_2H_4 + 25% CH_3OH flames at an axial height of 10 mm.

A comparison of some of the stable species profiles, in both ethene and ethene + methanol flames, as measured by gas-chromatography, are shown in Fig. 10. As observed, the concentration of C_2H_2, which is identified to be the most important growth species, remains fairly unaltered upon methanol addition. If we are to assume the measured C_4H_6 to be representative of n-C_4H_5 radical, a key component in the first ring formation, the observed reduction in C_6H_6 can be attributed to the reduced formation of the n-C_4H_5 radical. The lower C_6H_6 concentrations, in turn, could curtail the subsequent growth to larger aromatic molecules. As presented later, methanol also reduces soot formation in a base C_6H_6 flame. This suggests additional/alternative mechanisms to be in effect. Curtailment of H· superequilibrium as suggested earlier is likely.

CS_2 addition :

OH· fluorescence profiles upon CS_2 addition exhibit a different trend. At lower heights, the OH· concentrations are suppressed, while those at higher locations are increased with respect to the pure ethene flame (*cf.* Fig. 7). The decrease at lower heights may be explained by the production of the intermediate HSO_2, which catalyzes the H and OH radical recombination [31], according to

$$\begin{aligned} H + SO_2 + M &\leftrightarrow HSO_2 + M \\ H + HSO_2 &\leftrightarrow H_2 + SO_2 \\ OH + HSO_2 &\leftrightarrow H_2O + SO_2. \end{aligned} \qquad (8)$$

The fluorescence profiles of the small PAH species, upon CS_2 addition, could not be determined, mainly due to interferences from SO and SO_2 fluorescence. The fluorescence profiles of large PAH (*cf.* Fig. 9) show reductions greater than 80%. This may be explained, mainly based on the above radical recombination kinetics. A decrease in H· concentration could significantly curtail PAH formation [29].

Furthermore, sulfur appears to form strong C-S bonds on soot surfaces, which have been reported to be stable for temperatures up to 1200 K [32]. This process may decrease the number of chemically active sites on the soot surface which explains both, the observed higher OH· concentrations at higher locations, as well as, the observed decrease in surface growth rate as apparent from the measured profiles of f_v, N, and D_{63}.

The stable species profiles upon CS_2 addition appear to be different from those active for methanol addition. Most importantly, the concentrations of C_4H_6, whose concentration we associate with that of n-C_4H_5 radical, are reduced substantially (*cf.* Fig. 11). However, minimal reductions, merely 5%, are observed in C_6H_6 concentration. On the other hand, the peak in C_2H_2 concentration at 10mm occurs at larger radial positions. However, by 20 mm axial height, the [C_2H_2] profile shows little variation with that in the ethene flame. A similar trend is observed in C_3H_8 concentrations. As C_4H_x and C_3H_x radicals are believed to have very little contribution to surface growth, all of the above observations along with the large reductions in [PAH] suggest that C_4H_6, and hence n-C_4H_5, are related to PAH growth in these flames.

An alternative mechanism is the production of S radical upon CS_2 pyrolysis, which similar to the O radical, could oxidize the PAH species. Though, it is not very conclusive

as to which amongst the above mechanisms is the dominant one, it is certain that CS_2 interference to soot formation is largely chemical in nature.

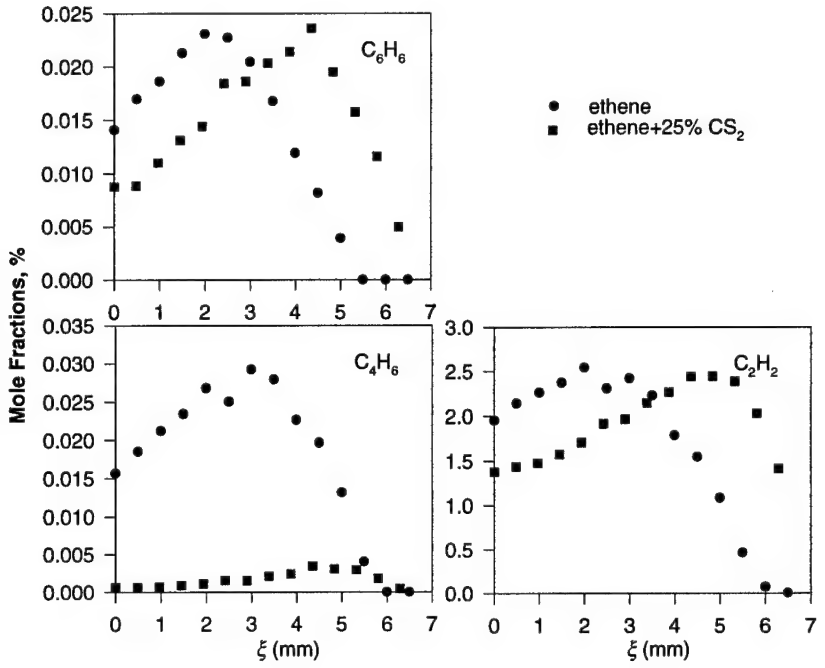

Figure 11. Stable species profiles in C_2H_4 and C_2H_4 + 25% CS_2 flames at an axial height of 10 mm.

3.4 Studies on Flames of High Energy Density Fuels

To check the effectiveness of CS_2 and CH_3OH in reducing soot in heavily sooting fuels, experiments were conducted with benzene (C_6H_6) and with a high energy density fuel, quadricyclane (C_7H_8). As both of these fuels are heavily sooting, a fuel mixture approach was adopted with methane as the base flame (flow conditions are shown in Table 5).

From comparisons as shown in Fig. 12, it can be observed that quadricyclane has a higher propensity to soot than benzene. Quadricyclane, being a highly strained molecule, is thermally unstable. Fuel pyrolysis of such a molecule is expected to result in early radical formation, which leads to an early initiation of the soot formation process. As benzene is relatively stable, it can be surmised that it initially follows a different chemical route to soot formation. However, in both the benzene and quadricyclane cases, appreciable soot reductions were observed with the addition of CH_3OH and CS_2.

Upon methanol addition, (*cf.* Fig. 13) it is observed that soot volume fraction, f_v, is reduced significantly for heights at or below 20 mm. However, higher in the flame soot reductions are comparably lower. The soot growth processes are found to overcome the soot suppression effects of methanol.

Table 5. Flow rates for high energy density fuel mixture flames

Name	Flow rates
C_6H_6	(CH_4 7.7 cm^3/s + C_7H_8 vap 0.1826 cm^3/s)-(CH_4 7.7 cm^3/s)
C_7H_8	(CH_4 7.7 cm^3/s + C_7H_8 vap 0.1626 cm^3/s)-(CH_4 7.7 cm^3/s)
CO_2/ C_7H_8	(CH_4 7.7 cm^3/s +CO_2 1.096 cm^3/s + C_7H_8 vap 0.1626 cm^3/s) -(CH_4 7.7 cm^3/s +CO_2 1.096 cm^3/s)
CS_2/ C_7H_8	(CH_4 7.7 cm^3/s +CS_2 1.096 cm^3/s + C_7H_8 vap 0.1626 cm^3/s) -(CH_4 7.7 cm^3/s +CS_2 1.096 cm^3/s)
CH_3OH/ C_7H_8	(CH_4 7.7 cm^3/s +CH_3OH vap 1.096 cm^3/s + C_7H_8 vap 0.1626 cm^3/s) -(CH_4 7.7 cm^3/s +CH_3OH vap 1.096 cm^3/s)

* Air flow rate for all the flames is 1060 cm^3/s; vap - indicates vapor flow rate.

Similar comparisons (*cf.* Fig. 14), indicate CS_2 to be very effective in reducing the sooting nature of these fuels; for 25% CS_2, soot reductions as large as 60% were observed. Similar to the observations made in C_2H_4 flames, very little soot forms at lower heights. As established in the case of ethene flames, influences upon CO_2 addition remain inconclusive. However, small soot reductions could be observed. Also, estimates of adiabatic flame temperatures (2200°C for $CS_2/C_7H_8/CH_4$, and 2217°C for $CO_2/C_7H_8/CH_4$ flames) show that the observed soot reductions cannot be due to a reduction in temperature. Overall, CS_2 seems to curtail soot formation better than methanol in the case of C_6H_6 and C_7H_8.

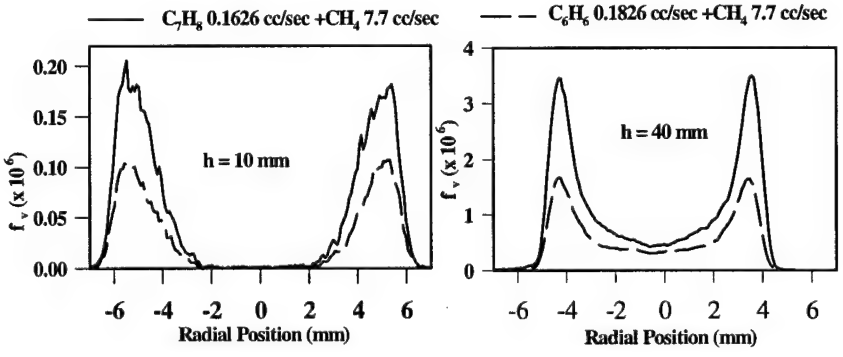

Figure 12. Soot profiles in C_6H_6 / CH_4 and C_7H_8 / CH_4 mixture flames.

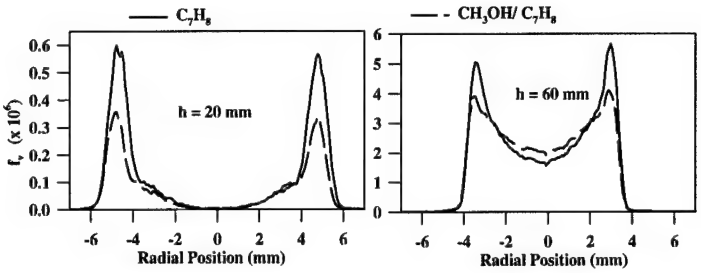

Figure 13. Soot volume fraction profiles with methanol addition to the quadricyclane /methane mixture flames for measurement heights, *h*, of 20 mm and 60 mm.

Our understanding about the processes associated with soot formation in quadricyclane are currently limited by the lack of knowledge of quadricyclane flame chemistry. Figure 15 compares the GC-FID traces for quadricyclane and ethene flames. Species specific to many of the peaks appearing in the case of quadricyclane could not be identified. In general, quadricyclane pyrolysis appears to result in the formation of large species (greater than C_3H_x), and is appreciably different from that of C_2H_4.

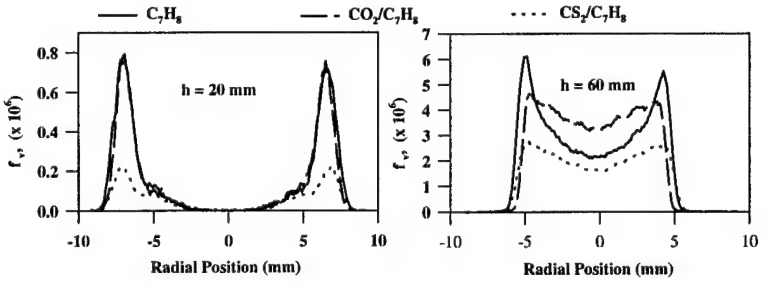

Figure 14. Soot volume fraction profiles with CS_2 addition to quadricyclane / methane mixture flames for measurement heights, *h*, of 20 mm and 60 mm.

3.5 Free Falling droplet Flame Studies

With an objective to evaluate the soot control strategies in spray environment, studies were conducted in free-falling droplet flames, as these flames easily lend themselves to experimental investigation. Additionally, since benzene is easily available and less expensive, it was used as a surrogate high energy density fuel. Subsequent studies performed on benzene / methanol blends are discussed in detail in Attachment B. Reductions in soot indices (grams of soot / drop) up to 90% were observed with 75% addition of methanol by liquid volume. In earlier stages, rapid preferential vaporization of less sooty methanol, and in later stages oxidant entrainment due to increased convection are believed to result in such reductions. Further details are presented in Attachment B.

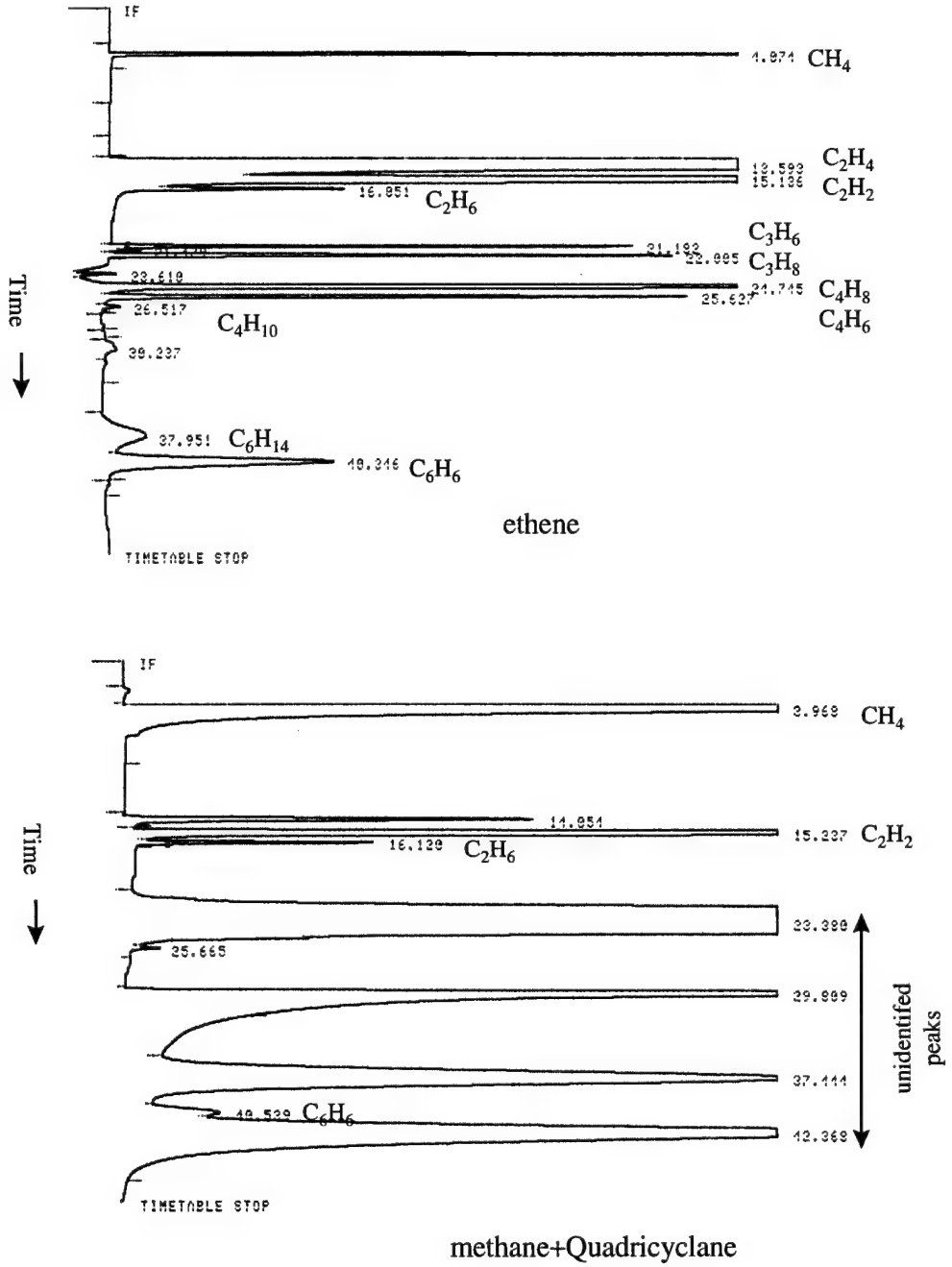

Figure 15. Comparison of FID output traces for quadricyclane and ethene flames obtained at 7 mm axial height along the centreline; the flow rates are (CH_4 7.7 cm^3/s + C_7H_8 vap 0.1626 cm^3/s), and 3.85 cm^3/s C_2H_4

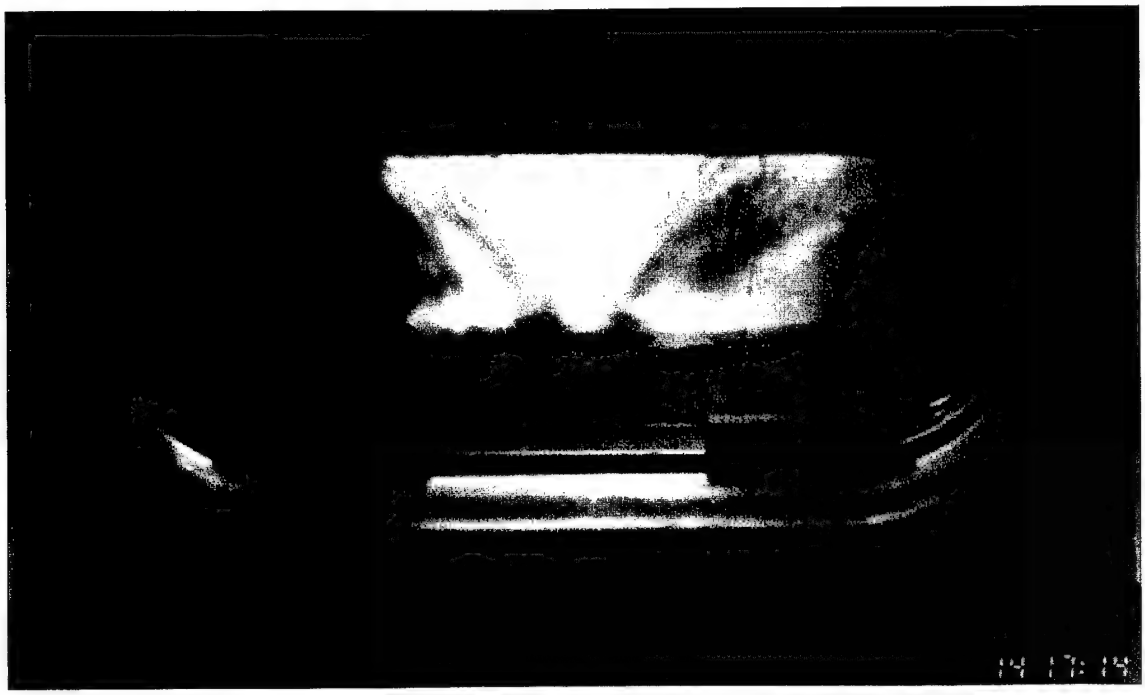

(a)

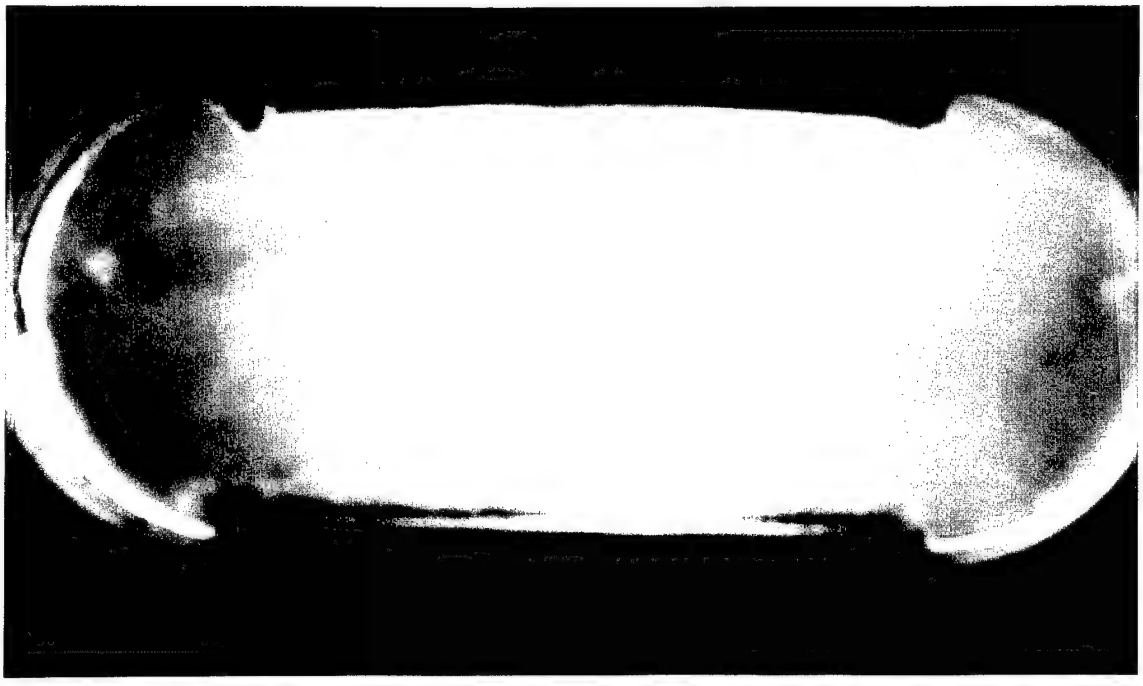

(b)

Figure. 16. Photographs of the luminosity of a spray flame produced by impinging jet atomizer. Chamber pressure is about 125 psia. (a) ethanol burning in oxygen, and (b) quadricyclane burning in oxygen.

CS_2 Addition

1) It is expected that most of the sulfur atoms in CS_2 are converted to SO_2. Subsequently, SO_2 forms the intermediate HSO_2 which catalyzes H, OH, and O radical recombination reactions [31], thereby reducing their concentrations close to their equilibrium values. As PAH formation and growth are sensitive to H radical concentrations [29], such effects are expected to profoundly affect net soot formation.

2) CS_2 upon pyrolysis results in the formation of sulfur radical, which similar to the O radical, could result in enhanced oxidation of PAH and acetylenic species.

3) As established by researchers in coal chemistry [32], stable C-S bonds could exist for temperatures up to 927°C. Such bonds, can lead to a decrease in the number of surface active sites, thereby leading to a curtailment of surface growth. However, further experimental evidence is sought to confirm the existence of such bonds at combustion temperatures.

The relative contributions of each of the above chemical mechanisms to the net soot reduction could not be evaluated through the present set of experiments. Future efforts should concentrate in such evaluations.

Similar studies, demonstrated carbon disulfide and methanol to be effective in controlling soot in both benzene (C_6H_6) and a high energy density fuel, quadricyclane (C_7H_8). Additional studies conducted on free falling droplet flames demonstrate the potential of methanol in curtailing soot formation in spray flames.

5.0 References

1) Law, C. K., Sixth ONR Propulsion meeting, Boulder, Colorado, pp. 25-29, 1993.
2) Moriarty, R. M. and Rao, M. S., Seventh ONR Propulsion Meeting, pp. 75-81, 1994.
3) Law, C. K., Seventh ONR Propulsion Meeting, pp. 110-116, 1994.
4) Howard, J. B. and Kausch Jr., W. J., *Prog. Energy Combust. Sci.*, vol. 6, pp. 263-276, 1981.
5) Salooja, K. C., *J. Inst. Fuel.*, Vol. 53, pp. 37-42, 1972.
6) Gulder, O. L., *Comb. and Flame*, Vol. 92, pp. 410 -418, 1993.
7) Du, D. X., Axelbaum, R. L., and Law, C. K., *Comb. and Flame*, Vol. 102, pp. 11 - 20, 1995.
8) Santoro, R. J., Semerjian, H. G., and Dobbins, R. A., *Comb. and Flame*, Vol. 51, pp. 203 - 218, 1983.
9) Kent, J. H., *Comb. and Flame*, Vol. 63, pp. 349 - 358, 1986.
10) Roper, F. G., *Comb. and Flame*, Vol. 29, pp. 227 - 234, 1977.
11) Quay, B., Lee, T. W., Ni, T., and Santoro, R. J., *Comb. and Flame*, Vol. 97, pp. 384 - 392, 1994.
12) Ni, T., Pinson, J. A., Gupta, S., and Santoro, R. J., *Applied Optics*, Vol. 34, No. 30, pp. 7083 - 7091, 1995.
13) Gupta, S. B., Ni, T., and Santoro, R. J., "Planar Imaging Applications in Sooting Turbulent Diffusion Flames," presented at the Fall technical meeting, The Eastern States Section of the Combustion Institute, 1995.
14) Kent, J. H. and Wagner, H. G., Twentieth Symposium (International) on Combustion, pp. 1007 - 1015, 1984.
15) Puri, R., Santoro, R. J. and Smyth, K. C., *Comb. and Flame*, Vol. 97, pp. 125 - 144, 1994.
16) Beretta, F., D'Alessio, A., D'orsi, A., and Minutolo, P., *Combustion Sci. Tech.* Vol. 85, pp. 455 - 470, 1992.
17) Puri, R., *Ph. D. Thesis, The Pennsylvania State University*, 1992.
18) Richardson, T., *Ph. D. Thesis, The Pennsylvania State University*, 1993.
19) Smyth, K. C., Tjossem, P. J., Hamins, A., and Miller, J. H., Combustion and Flame, vol. 79, pp. 366-380, 1990.
20) Ni, T., Gupta, S. B., and Santoro, R. J., *Twenty - Fifth Symposium (International) on Combustion*, pp. 585 - 592, 1994.
21) Berlman, I. B., *Handbook of Fluorescence of Aromatic Molecules*, Academic Press, New York, 1971.
22) D'Alessio, A., D'Anna, A., D'Orsi, A., Minutolo, P., Barbella, R., and Ciajolo, A., Twenty-Fourth Symposium (International) on Combustion, pp. 973-980, 1992.
23) Santoro, R. J. and Semerjian, H. G., *Twentieth Symposium (International) on Combustion*, pp. 997 - 1006, 1984.
24) Gomez, A., and Glassman, I., *Twenty - First Symposium (International) on Combustion*, pp. 1087, 1987.
25) Axelbaum, R. L., and Law, C. K., *Twenty - Third Symposium (International) on Combustion*, pp. 1517, 1991.

26) Santoro, R. J. and Richardson, T. F., *in "Soot Formation in Combustion," eds. H. Bockhorn, Springer series in Chemical physics*, pp. 221 - 238, 1994.
27) Westbrook, C. K. and Dryer, F. L., Combustion Science and technology, Vol. 20, pp. 125 - 140, 1979.
28) Glassman. I., *Personal communication*, 1995.
29) Frenklach, M. and Yuan, T., Sixteenth Symposium (International) on Shock Tubes and waves, pp. 487 - 493, 1987.
30) Alexious, A. and Williams, A., Combustion and Flame, Vol. 104, pp. 51 - 65, 1996.
31) Mueller, C. H., Schofield, K., Steinberg, M. and Broida, H. P., *Seventeenth Symposium (International) on Combustion*, pp. 867, 1978.
32) Sykes, K. W. and White, P., *Trans. Farady Soc.*, Vol. 52, pp. 660 - 671, 1956.

6.0 Publications

1) Ni, T., Pinson, J. A., Gupta, S. B., and Santoro, R. J., "Two-Dimensional Imaging of Soot-Volume Fraction Using Laser-Induced Incandescence," *Applied Optics,* vol. 34, No.30, Oct 1995, pp. 7083 - 7091.

2) Gupta, S. B., Ni, T., and Santoro, R. J., "Planar Imaging Applications in Sooting Turbulent Diffusion Flames," *Fall Technical Meeting, The Eastern States Section of the Combustion Institute*, Oct. 1995.

3) Gupta, S. B., Ni, T., and Santoro, R. J., "Reduction of Soot Formation in High Energy Density Fuels," 32nd *JANNAF Combustion Subcommittee /PERC meeting*, NASA Marshall Space Flight Center, Huntsville, AL, Oct. 1995.

4) Gupta, S. B. and Santoro, R. J., "Spatial and time-resolved soot-volume fraction measurements in methanol/benzene droplet flames," *Fall Technical meeting, The Eastern States Section of the Combustion Institute*, Dec. 1994.

5) Ni, T., Gupta, S. B., and Santoro, R. J., "Suppression of Soot Formation in Ethene Laminar Diffusion Flames by Chemical Additives" *Twenty-Fifth Symposium (International) on Combustion, The combustion Institute*, 1994, pp. 585-592.

7.0 Personnel

R. J. Santoro	Professor of Mechanical Engineering
T. Ni	Post-doctoral Fellow
S. B. Gupta	Graduate student (Ph.D. completion October 1996)
S-Y. Lee	Graduate student
W. E. Anderson	Post-doctoral Fellow
D. Boone	Technician
T-W. Lee	Post-doctoral Fellow

Attachment A

Suppression of Soot Formation in Ethene Laminar Diffusion Flames by Chemical Additives

by

T. Ni, S. B. Gupta, and R. J. Santoro

Twenty-Fifth Symposium (International) on Combustion
The Combustion Institute
1994, pp. 585-592.

Twenty-Fifth Symposium (International) on Combustion/The Combustion Institute, 1994/pp. 583–592

SUPPRESSION OF SOOT FORMATION IN ETHENE LAMINAR DIFFUSION FLAMES BY CHEMICAL ADDITIVES

T. NI, S. B. GUPTA AND R. J. SANTORO
Department of Mechanical Engineering
The Pennsylvania State University
University Park, PA 16802, USA

The effects of methane, methanol, ethanol, 1-propanol, 2-propanol, carbon dioxide, and carbon disulfide addition on soot formation in ethene laminar diffusion flames were examined. In this study, one-dimensional (1D) laser-induced incandescence (LII) and fluorescence measurements were used to determine soot volume fraction and relative soot precursor concentration, respectively, in the ethene and (ethene + additive) flames. Up to 60% reductions in soot volume fraction were found with the addition of 25% methanol to an ethene diffusion flame. More significant soot reductions were observed with the addition of carbon disulfide. It has been shown that a more than 50% reduction in soot volume fraction was achieved by adding 9.5% CS_2. Experimental results strongly suggest suppression of soot formation by methanol and carbon disulfide to be mainly a chemical effect.

Introduction

The ramifications of soot formation on the environment, public health, and hardware performance in practical combustion systems have long been identified. The current need for understanding and control of soot formation stems from the future increase in the aromatic content of commercial fuels, as well as the prospect of stricter environmental standards. One of the practical approaches to soot reduction is to blend additives into the fuel, so as to alter the soot nucleation and growth processes or to enhance soot oxidation.

Although the effects of various additives on soot formation have been observed by numerous researchers, relatively little is known about the mechanisms involved in soot suppression. Phenomenological theories have been suggested to explain the influence of additives on the formation of soot particles. For example, modest reductions in soot loading in diffusion flames by addition of inert species, such as Ar and N_2, have largely been attributed to lower flame temperatures and decreased fuel concentrations (dilution) [1–3]. Such effects are believed to significantly decrease the reaction rates of processes leading to soot formation. However, large reductions in soot formation by additives have been explained by chemical mechanisms. Soot suppression by alcohol addition has been observed both in shock tubes [4,5] and in flames [6]. Frenklach and Yuan [4], in studies of the effects of methanol and ethanol addition to benzene on soot formation, have attributed the suppression effect to enhanced oxidation of soot and soot precursors by OH generated from alcohol pyrolysis and removal of hydrogen atoms. The most effective gaseous soot suppression additives appear to be sulfur compounds, such as H_2S [7], SF_6 [8], and SO_2 [7,9]. It has been suggested that SO_2 promotes the oxidation of soot precursors and soot particles, probably due to increased OH concentration [10]. Calder [11], however, reports that for mole fractions less than 40%, SO_2 has no direct chemical influence on soot formation, and the soot reduction observed is purely due to lower flame temperature and fuel concentration. Randolph and Law [12], based on studies involving the addition of propanol and hexanol to hydrocarbon droplet studies, question the role of the hydroxyl group of alcohol in soot suppression. They have reported that the addition of alcohol reduces soot by the same amount as other soot-controlling additives, indicating the dilution of the fuel concentration to be the dominant factor in soot reduction with no observable chemical effect [12].

The present study was undertaken to examine the importance of chemical effects when soot-suppressant additives, such as methanol and carbon disulfide, are introduced into ethene diffusion flames. A series of controlled experiments were performed to isolate such effects.

Experimental Approach

In these experiments, a laminar diffusion flame was established using a coannular burner, which consists of a 1.1-cm-diameter fuel tube surrounded by a 10.2-cm-diameter air tube [13]. A 40.5-cm-long brass cylinder was used as a chimney to shield the flame from laboratory air currents. Two holes diametrically

TABLE 1
Flow conditions and calculated adiabatic temperatures[a] (T_{ad}) of ethene-additive mixture diffusion flames

Flame No.	Fuel (cm³/s)	Additive (cm³/s)[b]	Mole% of additive	C% of additive	T_{ad} (K)
1	C_2H_4 (3.85)				2370
2	C_2H_4 (3.30)	CH_4 (1.10)	25.0	14.2	2345
3	C_2H_4 (3.30)	CH_3OH (1.10)	25.0	14.2	2347
4	C_2H_4 (3.08)	CH_4 (1.54)	33.3	20.0	2336
5	C_2H_4 (3.08)	CH_3OH (1.54)	33.3	20.0	2338
6	C_2H_4 (3.08)	C_2H_5OH (0.77)	20.0	20.0	2343
7	C_2H_4 (3.30)	1-C_3H_7-OH (0.37)	10.1	14.2	2353
8	C_2H_4 (3.30)	2-C_3H_7-OH (0.37)	10.1	14.2	2352
9	C_2H_4 (3.66)	CS_2 (0.38)	9.5	5.0	2361
10	C_2H_4 (3.30)	CS_2 (1.10)	25.0	14.2	2346
11	C_2H_4 (3.30)	CO_2 (1.10)	25.0	14.2	2328

[a]Calculated using NASA Chemical Equilibrium Code.
[b]Vapor flow rate.

opposite and 0.8 cm in diameter were used for passing the laser beam through the flame. Another 5 × 5 cm slot covered with a quartz plate provided optical access for the emitted light. The air and gaseous fuel flows to the burner were metered with calibrated rotameters. Liquid additives, which were supplied by a precision syringe pump, were vaporized and mixed with the fuel in a vaporizer. The temperature of the vaporizer was maintained to within 5 °C of the boiling point of the liquid additives. To prevent any condensation of the liquid additives, the fuel line and fuel tube were heated with a heating wire. By varying the electric voltage applied to the heating wire, the temperature of the fuel flow at the lip of the burner was maintained at 60 °C for all fuel mixtures regardless of whether a liquid additive was introduced. This approach ensures that all the flames were established at the same ambient condition.

Flames burning ethene (CP grade, 99.5%) mixed with methane (CP grade, 99%), methanol (HPLC grade, 99.5%), ethanol (CP grade, 99%), 1-propanol (HPLC grade, 99.5%), 2-propanol (HPLC grade, 99.5%), carbon dioxide (bone dry grade, 99.8%), and carbon disulfide (HPLC grade, 99.5%) were studied. When an additive was introduced into the fuel line, the ethene flow rate was reduced in appropriate proportion in order to keep the total carbon flow rate constant. This ensures similar flame sizes and shapes. The air flow rate was maintained at 1060 cm³/s for all flames. Table 1 summarizes the flow conditions and calculated adiabatic flame temperatures for the flames studied.

Laser-induced incandescence (LII) was applied to obtain spatial distribution of soot volume fraction (f_v) in the flames. The one-dimensional (1D) LII technique employed here is a modification of the technique followed by Quay et al. [14], where these authors have made point measurements while using a calibration scheme to measure local soot volume fraction quantitatively.

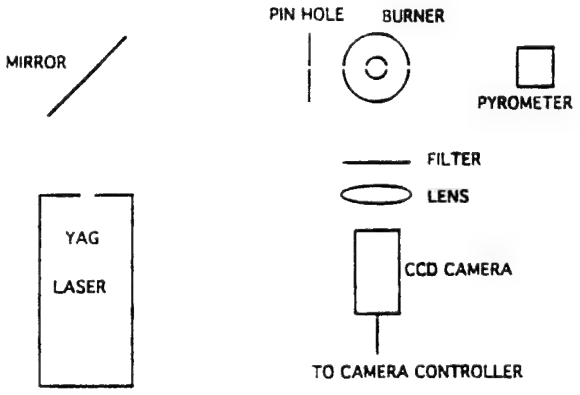

FIG. 1. Schematic diagram of 1D laser-induced incandescence experimental setup.

The optical setup for these measurements is given in Fig. 1. A Nd:YAG pulsed laser (Surelite, Continuum) operating at 10 Hz was used as an intense light source. A 1-mm-diameter pinhole was placed in front of the burner, which allowed only the center portion of the 6-mm-diameter laser beam to heat the soot particles. Diffraction effects were minimized by placing the pinhole as close as possible to the flame. In such a practice, the center portion of the near Gaussian beam is virtually uniform and intense enough to heat the soot particles to their vaporization temperature without additional focusing. Since the beam is unfocussed, the beam size across the flame is virtually constant, thus, eliminating the error associated with the change in the probe volume across the beam in

a 1D measurement. Both the 1064 nm and frequency-doubled 532-nm beams were used in this experiment. Comparison of 1064 and 532 nm excitation showed no significant difference on 1D LII profiles obtained for the ethene flames, although the use of 1064-nm beam showed certain advantages in penetrating heavily sooting flames. The laser beam behind the pinhole was monitored and maintained at 1.5 mJ/pulse, which corresponds to an average light fluence of 2.5×10^7 W/cm^2 for 8-ns full width at half-maximum (FWHM) laser pulse. The induced incandescence at a 90° angle was imaged with a 105-mm UV camera lens (Nikon, f/4.5) onto an intensified charge coupled device (CCD) camera (Princeton Instruments, Model ICCD-576S/RB). The camera was gated-on immediately after the laser pulse for 18 ns. A narrow band interference filter (transmittance centered at 460 nm) was placed in front of the camera to prevent light scattering from soot particles by the laser beam from reaching the detector and to reject most background luminosity and laser-induced fluorescence. Laser-induced incandescence images were acquired by averaging over 40 laser pulses. A calibration factor was used to obtain absolute local soot volume fraction. Measurements made using a light extinction/scattering technique on a well-established ethene laminar diffusion flame provided the calibration factor [13]. The uncertainties in the soot volume fractions derived from the 1D LII measurements were less than 5%.

The effect of the additives on soot precursor formation was assessed using laser-induced fluorescence measurements attributed to polycyclic aromatic hydrocarbon (PAH) species formed in the flames. The association of similar broadband laser-induced fluorescence, observed in both premixed and diffusion flames, with PAH species has been reported in the past [15–19]. Some controversy remains regarding the correspondence between this broadband fluorescence and PAH species since the direct association of the observed fluorescence with specific PAH species has not been unambiguously established. Thus, there is the possibility that other large hydrocarbon species such as polyenes and polyynes can contribute to the observed fluorescence. Nonetheless, we argue that variations in the concentrations of these species would also reflect the overall hydrocarbon kinetics that characterize the soot precursor evolution. Furthermore, it should be noted that the PAH species responsible for the fluorescence signals may not be soot precursors themselves, but rather they could be byproducts formed along the reaction route to soot particles. Again, in this work their concentration is argued to follow proportionally the soot precursor formation process. With these assumptions stated, the observed fluorescence variations are used in the present study to infer effects on soot precursors in the flames caused by the introduction of additives.

The optical setup for 1D PAH fluorescence imaging is very similar to that used for LII measurements, except that the excitation energy is much lower (<50 μJ/pulse). Since the spectra of both LII [14] and PAH [18] fluorescence are broadband in nature, it is difficult to isolate the fluorescence signal from LII emission. In this experiment, the excitation laser energy was kept below the LII threshold so that only the fluorescence, which is linear with laser fluence, was observed. The excitation sources are a Nd:YAG laser operated at 532 nm for the detection of large PAH and a Nd:YAG pumped dye laser with frequency doubling to 290 nm for the detection of small PAH. The laser, when operated at the 532-nm wavelength, excites only PAH molecules that contain roughly more than 5 aromatic rings [20], whose emission at 650 ± 10 nm was measured. The UV beam of 290 nm excites both large and small PAH molecules. By placing a combination of a 305-nm cutoff filter (WG305) and a UV-pass filter (UG11) in the front of the camera, only the emission ranging from 305 to 380 nm, which corresponds to small PAH molecules (approximately less than 5 rings), was captured. The camera was gated-on for 5 ns during the laser pulse. Fluorescence from 200 laser pulses were accumulated to generate a 1D fluorescence intensity profile.

The fluorescence lifetime for the PAH species was measured in the flame and observed to be approximately 30 ns in duration. The fluorescence lifetime for these species in the absence of collisional quenching is expected to be about 200 ns [20]. Thus, collisional quenching reduces the fluorescence lifetime by only an order of magnitude. Then, for the present conditions, quenching reduces the fluorescence lifetime rather than reducing the number of excited molecules. Thus, the effects of collisional quenching can be minimized by detecting the fluorescence during the laser pulse using an appropriately short gate width as was the procedure in the present experiments. The fluorescence intensity, therefore, was not corrected for collisional quenching, and the fluorescence is argued to be linearly proportional to the PAH concentration at approximately equivalent locations in the flame. From the measurements of the fluorescence lifetime for these species, we estimate that a change in the collisional quenching of a factor of 2 would only change the measured fluorescence by ±10% or less.

The temperature distribution measurements were made using the rapid insertion thermocouple technique similar to that described by Kent and Wagner [21]. In this technique, the soot deposited on the thermocouple surface is burned off in the oxidation zone of the flame prior to making a measurement at a new location. The uncoated Pt/Pt-10% Rh thermocouple was made from 127-μm-diameter fine wires. The temperature measurements were not corrected for radiation effects. Nonetheless, this tech-

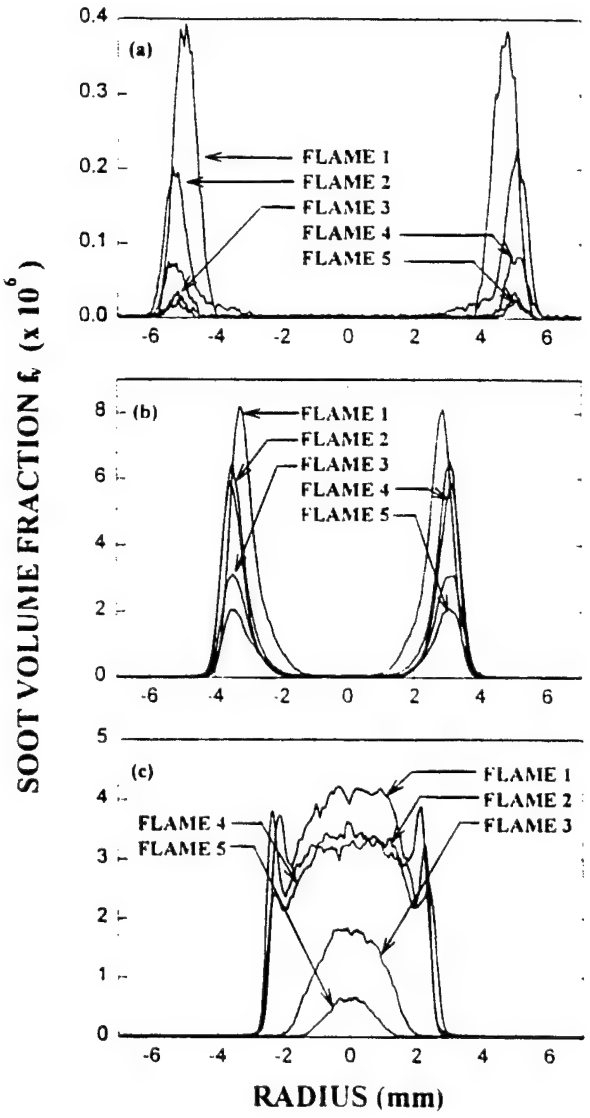

FIG. 2. Soot volume fraction profiles in the pure ethene diffusion flame (flame 1) and the flames mixed with 14.2 C% methane (flame 2), 20 C% methane (flame 4), 14.2 C% methanol (flame 3), and 20 C% methanol (flame 5): (a) 7-mm height; (b) 30-mm height; (c) 60-mm height.

nique provides accurate measurement of relative temperature changes.

Results and Discussion

Alcohol Addition:

Figure 2 shows the radial soot volume fraction profiles at three heights in the flames. The addition of 25% methanol (14.2 C%, flame 3) reduces the soot concentration by 60%, at least for all axial locations. Such strong reductions in soot loading suggest that chemical effects may be involved in the suppression of soot formation by methanol. In order to differentiate the chemical effects from dilution and temperature effects resulting from methanol addition, an ethene/methane mixture (which does not have an OH group, flame 2) was used for comparison. The comparison of the effect of methanol addition with methane addition on soot volume fraction f_v, as shown in Fig. 2, reveals that methanol addition reduces f_v substantially, as compared to methane addition. The difference between methanol addition and methane addition cannot be attributed to additional soot formed from methane because the soot concentration in a pure methane diffusion flame [2] is less than a twentieth of that in the ethene flame. Previous studies of laminar diffusion flames indicate that lowering flame temperature can significantly reduce soot formation [1–3]. However, this thermal effect was ruled out, since the calculated adiabatic temperature of ethene/methanol flames closely matches that of the ethene/methane flames (see Table 1). In fact, the ethene/methanol flame temperature in the soot inception zone, as measured by a thermocouple, is 10 °C higher than in the ethene/methane flame due to less radiative heat loss. These observations strongly suggest that a chemical interaction is the dominant effect in soot suppression by methanol addition.

In order to gain further insight into the chemical processes leading to soot reduction, measurements of PAH fluorescence were obtained in ethene, ethene/methanol, and ethene/methane flames. Polycyclic aromatic hydrocarbon species are often viewed as precursors to soot particles [22] and are a possible source of mass for soot growth [23]. As it is difficult to quantify the quenching effect and thermal effect on fluorescence intensity, absolute PAH concentration measurements were not obtained. However, in diffusion flames, the concentration of oxygen, which strongly quenches the fluorescence of most organic compounds, is negligible in the PAH formation zone, and the temperature profiles of the ethene/methanol and ethene/methane flames are very close to each other. Thus, PAH fluorescence measurements can provide information about the relative change of PAH concentration. Figure 3 shows radial profiles of PAH fluorescence intensity taken at a height of 10 mm above the fuel tube exit for ethene, ethene/methanol, and ethene/methane flames. It is interesting to note that the fluorescence intensities of larger PAH species excited by the 532-nm-wavelength laser beam achieve their maximum slightly further away from the centerline as compared to the profiles of smaller PAH species. A similar result has been previously reported by Smyth et al. [24] for Wolfhard–Parker slot burner studies of methane diffusion flames. Comparison of fluorescence profiles in ethene/methanol and ethene/methane flames indicates that the fluorescence intensities of both large and small PAH species are lower in the ethene/methanol flame. These results support an argument that the addition of methanol reduces the formation of soot

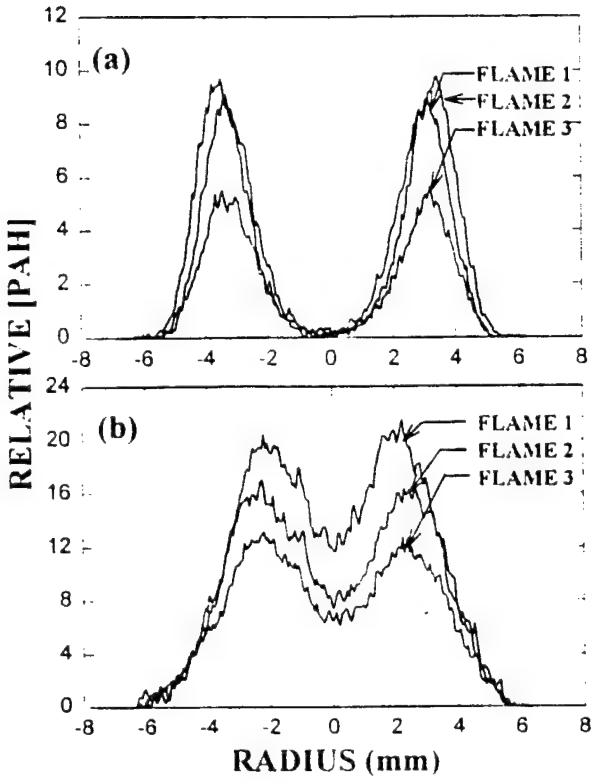

FIG. 3. Comparison of PAH fluorescence intensities of the pure ethene flame (flame 1) and the flames mixed with 14.2 C% methane (flame 2) and 14.2 C% methanol (flame 3) at the 10-mm height: (a) excited at a wavelength of 532 nm, (b) excited at a wavelength of 290 nm.

particles by retarding the formation of the key soot precursors or oxidizing them through OH attack.

In order to further understand the role of the hydroxyl group in alcohols, three other alcohols (ethanol, 1-propanol, and 2-propanol) have been added to an ethene laminar diffusion flame. Figure 4 shows the radial soot volume fraction (f_v) profiles at the 40-mm axial location of the flames. Comparison with the pure ethene flame illustrates that not all alcohols are equally effective in soot suppression. Methanol was observed to reduce soot significantly, while ethanol and propanol have much less of an effect on the soot concentration. Indeed, 1-propanol and 2-propanol were found to slightly increase soot concentration. Since ethanol is a nonsooting fuel, this result reveals that the dilution effect, i.e., the reduction of soot concentration by diluting a sooting fuel with a nonsooting fuel species, is not significant in reducing f_v in the present studies. It should be noted that these results are consistent with the fact that the pyrolysis of methanol [25] generates OH radicals, which can oxidize soot particles or soot precursors, while the main pyrolysis product of ethanol [26] is ethene and water. In droplet flame studies, Randolph and Law found that the hydroxyl group in hexanol has no effect on soot concentration [12]. A possible explana-

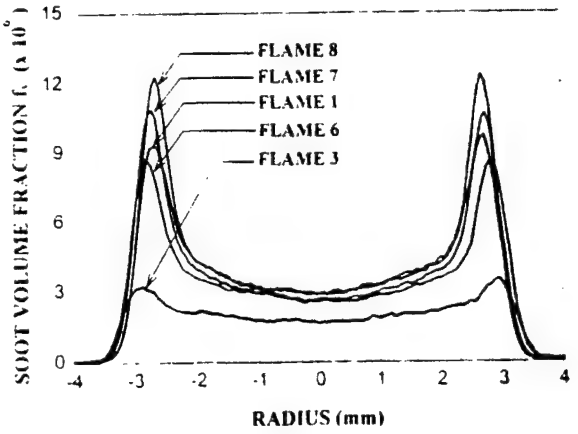

FIG. 4. Comparison of soot volume fraction profiles of the pure ethene flame (flame 1) and the flames mixed with 14.2 C% methanol (flame 5), 20 C% ethanol (flame 6), 14.2 C% 1-propanol (flame 7), and 14.2 C% 2-propanol (flame 8) at the 40-mm height.

tion is that hexanol, like ethanol, does not produce a significant amount of OH radicals during pyrolysis.

Frenklach and Yuan [4] suggested a hydrogen removal mechanism to explain the effect of alcohol addition on soot formation. In their mechanism, hydrogen atoms were removed through the following reactions:

$$H + ROH \rightarrow H_2 + RO \quad (1)$$

$$H + ROH \rightarrow H_2 + R'OH \quad (2)$$

$$H + ROH \rightarrow OH + RH. \quad (3)$$

Hydrogen atoms are believed to play a key role in the production of reactive radical species in the formation of soot precursors [27]. Removal of hydrogen atoms should slow down the reactions toward soot formation. However, the lack of soot reduction by 1-propanol and 2-propanol addition does not support this mechanism as a general explanation for the effects of all alcohols.

Carbon Disulfide Addition:

During the combustion of fuel with carbon disulfide as an additive, Sye and Hwang observed a marked decrease in the formation of polycyclic aromatic hydrocarbons [28], the intermediates for soot particle formation. In the pyrolysis processes of hydrocarbons, carbon disulfide has been used to minimize the formation of coke [29]. In present work, CS_2 was added to ethene diffusion flames to study the chemical influence of CS_2 on soot formation. Figure 5 shows LII measurements at three heights above the burner for ethene, ethene/CS_2 and ethene/CO_2 flames. These profiles reveal that at lower

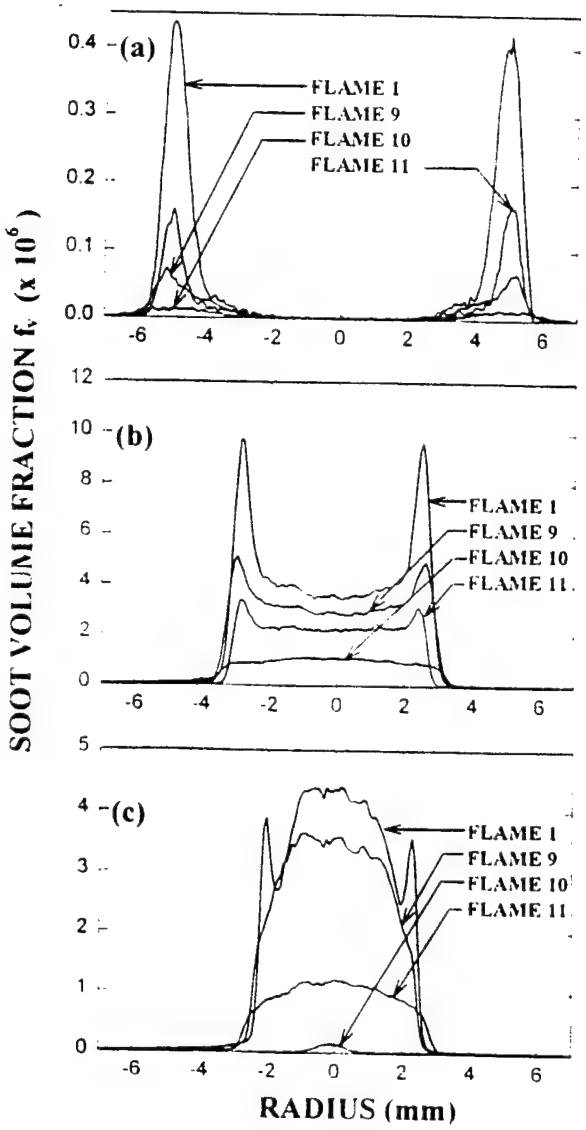

FIG. 5. Soot volume fraction profiles of the pure ethene flame (flame 1) and the flames mixed with 5.0 C% carbon disulfide (flame 9), 14.2 C% carbon disulfide (flame 10), and 14.2 C% carbon dioxide (flame 11): (a) 7-mm height, (b) 40-mm height, (c) 60-mm height.

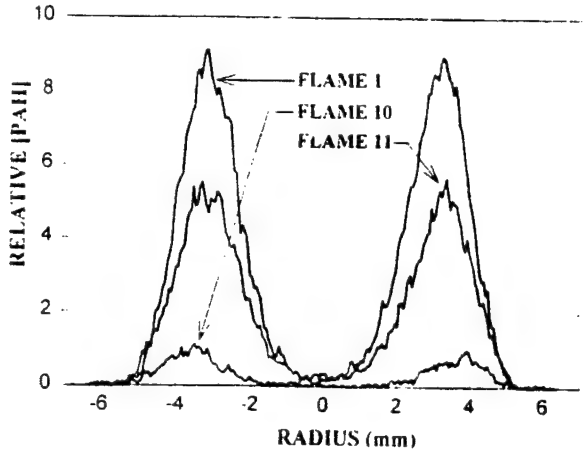

FIG. 6. PAH fluorescence intensity profiles of the pure ethene flame (flame 1) and the flames mixed with 14.2 C% carbon dioxide (flame 11) and 14.2 C% carbon disulfide (flame 10) at 10-mm height excited at a wavelength of 532 nm.

heights in the flame, the addition of 9.5 and 25% CS_2 (5.0 and 14.2 C%, respectively) substantially reduces the formation of soot. For the purpose of comparison, carbon dioxide was introduced into the ethene diffusion flame and a considerable reduction of soot was observed. This reduction may be due to lower adiabatic flame temperature (listed in Table 1), dilution, and chemical effects [30,31]. Although the adiabatic temperatures of ethene/CS_2 flames are higher than ethene/CO_2 flames with the same fuel-to-additive ratio, the soot volume fraction in ethene/CS_2 flames was substantially lower than that in the ethene/CO_2 flame at low heights. These results lead to the conclusion that a chemical effect due to the addition of CS_2 is important in soot suppression observed, and this chemical effect in the lower part of the flame is stronger than the effects due to CO_2 addition.

However, higher in the flames, the influence on soot concentration by CS_2 addition becomes less effective. At 60 mm above the burner, the soot volume fraction in the ethene + 25% CS_2 (14.2 C%) flame is observed to be higher than in the ethene + 25% CO_2 (14.2 C%) flame. A possible explanation for this observation is that the addition of CS_2 retards the formation and growth of soot particles rather than enhancing soot burnout. Recently, Gulder reported that the addition of less than 40% SO_2 does not have a chemical influence on soot concentration in diffusion flames [11]. Considering CS_2 oxidation to SO_2 in the oxidation zone of the diffusion flame and the lack of burnout enhancement, our results are consistent with Gulder's observation.

The measurements of PAH fluorescence further confirm the conclusion that the chemical interaction of CS_2 is significant. As shown in Fig. 6, the addition of 25% CS_2 (14.2 C%) reduces the fluorescence intensity of large PAH species by more than 90%. As a comparison, the same amount of CO_2 reduces fluorescence intensity by 40%. The mechanism involving the chemical interaction is not known yet. But it is expected that sulfur atom, an oxidizing species, is generated during the pyrolysis of CS_2 and may participate in the destruction of aromatic hydrocarbons similar to OH radical. The absorption of sulfur on soot particle surface may also slow down the rate of soot growth. It has been reported that sulfur and carbon disulfide can chemically bond to active sites on the carbon surface [32]. The resulting carbon-sulfur surface compound is extremely stable at 700 °C [33] and still exists at temperatures up to 927 °C [34,35]. It might be possible that the formation of such sur-

face compounds reduces the number of active carbon sites on soot surface, thus, preventing continuous growth of the soot particles. However, to date, no experimental evidence is available to support the existence of such a surface compound in the soot growth regions where temperatures as high as 1200 °C exist. Further investigation is needed to confirm this hypothesis.

Conclusions

1. It was demonstrated that the addition of methanol and CS_2 into ethene diffusion flames can significantly reduce the formation of soot particles.
2. Chemical interaction was found to play an important role in the suppression of soot formation by methanol and carbon disulfide addition.
3. Measurements of fluorescence from polycyclic aromatic hydrocarbons in ethene diffusion flames indicate that these species are reduced significantly by methanol and CS_2 addition.

Acknowledgment

Funding for this work from the Office of Naval Research under Grant No. N00014-93-0185 with Dr. Gabriel D. Roy as contract monitor is gratefully acknowledged.

REFERENCES

1. Schug, K. P., Manheimer-Timnat, Y., Yaccarino, P., and Glassman, I., *Combust. Sci. Technol.* 22:235–250 (1980).
2. Santoro, R. J. and Semerjian, H. G., *Twentieth Symposium (International) on Combustion*, The Combustion Institute, Pittsburgh, 1984, pp. 997–1006.
3. Axelbaum, R. L., Flower, W. L., and Law, C. K., *Combust. Sci. Technol.* 61:51–73 (1988).
4. Frenklach, M., and Yuan, T., *Sixteenth International Symposium on Shock Tubes and Waves*, Aachen, West Germany, 1987, pp. 487–493.
5. Alexiou, A., Williams, A., and Abdalla, A. Y., *Prepr. Am. Chem. Soc. Div. Fuel Chem.* 36:1547–1554 (1991).
6. Kadota, T., and Hiroyasu, H., *Combust. Flame* 55:195–201 (1984).
7. Haynes, B. S., Jander, H., Matzing, H., and Wagner, H. Gg., *Nineteenth Symposium (International) on Combustion*, The Combustion Institute, Pittsburgh, 1982, pp. 1379–1385.
8. Mitchell, J. B. A., and Miller, D. J. M., *Combust. Flame* 75:45–55 (1989).
9. Lawton, S. A., *Combust. Flame* 75:175–181 (1989).
10. Cotton, D. H., Friswell, N. J., and Jenkins, D. R., *Combust. Flame* 17:97–98 (1971).
11. Gulder, O. L., *Combust. Flame* 92:410–418 (1993).
12. Randolph, A. L., and Law, C. K., *Twenty-First Symposium (International) on Combustion*, The Combustion Institute, Pittsburgh, 1986, pp. 1125–1131.
13. Santoro, R. J., Semerjian, H. G., and Dobbins, R. A., *Combust. Flame* 51:203–218 (1983).
14. Quay, B., Lee, T.-W., Ni, T., and Santoro, R. J., *Combust. Flame* 97:384–392 (1994).
15. Coe, D. S., Haynes, B. S., and Steinfeld, J. L., *Combust. Flame* 43:211–214 (1981).
16. Miller, J. H., Mallard, W. G., and Smith, K. C., *Combust. Flame* 47:205–214 (1982).
17. Prado, G., Garo, A., Ko, A., and Sarofim, A., *Twentieth Symposium (International) on Combustion*, The Combustion Institute, Pittsburgh, 1985, pp. 989–996.
18. Beretta, F., Cincotti, V., D'Alessio, A., and Menna, P., *Combust. Flame* 61:211–218 (1985).
19. Petarca, L., and Marconi, F., *Combust. Flame* 78:308–325 (1989).
20. Berlman, I. B., *Handbook of Fluorescence of Aromatic Molecules*, Academic Press, New York, 1971.
21. Kent, J. H., and Wagner, H. Gg., *Combust. Sci. Technol.* 41:245–269 (1984).
22. Haynes, B. S., and Wagner, H. Gg., *Prog. Energy Combust. Sci.* 7:229–273 (1981).
23. McKinnon, J. T., and Howard, J. B., *Twenty-Fourth Symposium (International) on Combustion*, The Combustion Institute, Pittsburgh, 1992, pp. 965–971.
24. Smyth, K. C., Miller, J. H., Dorfman, R. C., Mallard, W. G., and Santoro, R. J., *Combust. Flame* 62:157–181 (1985).
25. Cribb, P. H., Dove, J. E., and Yamazaki, S., *Twentieth Symposium (International) on Combustion*, The Combustion Institute, Pittsburgh, 1985, pp. 779–787.
26. Rotzoll, G., *J. Anal. Appl. Pyrolysis* 9:43–52 (1985).
27. Frenklach, M., Clary, D. W., Gardiner, W. C., Jr., and Stein, S. E., *Twentieth Symposium (International) on Combustion*, The Combustion Institute, Pittsburgh, 1985, pp. 887–901.
28. Sye, W. F., and Hwang, S. S., *J. Chin. Chem. Soc.* 36:235–240 (1989).
29. Bajus, M., and Baxa, J., *Collect. Czech. Chem. Commun.* 50:2903–2909 (1985).
30. Du, D. X., Axelbaum, R. L., and Law, C. K., *Twenty-Third Symposium (International) on Combustion*, The Combustion Institute, Pittsburgh, 1991, p. 1509.
31. Zhang, C., Atreya, A., and Lee, K., *Twenty-Fourth Symposium (International) on Combustion*, The Combustion Institute, Pittsburgh, 1992, pp. 1049–1057.
32. Blayden, H. E., and Patrick, J. W., *Carbon* 5:533–544 (1967).
33. Chang, C. H., *Carbon* 19:175–186 (1981).
34. Sykes, K. W., and White, P., *Trans. Faraday Soc.* 52:660–671 (1956).
35. Owen, A. J., Sykes, K. W., Thomas, D. J. D., and White, P., *Trans. Faraday Soc.* 49:1198–1206 (1953).

COMMENTS

Omer L. Gülder, National Research Council, Canada. I have two comments and a question. The first comment is that in our experiments with liquid hydrocarbon fuels (mixtures of isooctane and toluene), the addition of methanol has not caused as much suppression as you observed in ethene flames. The behavior of ethene may not be typical of higher hydrocarbons. The second comment is related to the chemical influence of methanol addition on the soot formation process. In the pyrolysis of methanol, acetylene concentrations are very small as compared with those observed in methane pyrolysis. This could be one of the possible reasons that methanol addition suppresses soot formation more than methane does.

My question is whether you observed any changes in the visible flame height when you introduced the additives to the fuel side. If you did, then the comparison of the soot concentrations at the same downstream flame location would not be meaningful.

Author's Reply. Regarding your first comment, the difference between your results with liquid hydrocarbon fuels and our gas phase studies may be due to fuel volatility effects [1]. In our experiments, the added concentration of methanol was controlled directly, whereas in liquid fuel studies, the relative volatility of the fuel mixture components will determine how much methanol is vaporized and when the vaporization occurs during the combustion process [1]. Thus, our two studies may not be directly comparable as to the effectiveness of methanol addition on soot reduction.

As to your second comment, we would agree that acetylene is an important intermediate species in soot formation. The specifics of the chemical mechanism by which soot formation is reduced in this study have not been specifically identified.

The flame height in these studies varied from 87 mm for the pure C_2H_4 flame to 67 mm for C_2H_4/20% CH_3OH flame. However, the residence time to reach a specific height in the flame does not change in these buoyancy-dominated laminar diffusion flames, particularly under the conditions used in this study of maintaining a constant carbon atom volume flow rate. Thus, comparisons at similar heights represent comparable residence times, which we believe is an appropriate basis from which to compare the effects of the additives.

REFERENCE

1. Randolph, A. L., and Law, C. K., *Combust. Flame* 64:267–284 (1986).

•

Rudolf R. Maly, Daimler Benz, Germany. Your results suggest that addition of sulfur compounds to fuels reduces soot. In diesel engines it is well known that minute quantities of sulfur compounds increase soot emission. Would you please elaborate on these controversial results? Or do your results have no relation to soot in practical combustion systems?

Author's Reply. The reduction of particulate emissions from diesel engines as sulfur content of the fuel decreases is well known, as you point out. However, tail pipe particulate emissions from diesel engines include soot particles and species that condense on the soot particles. The reduction in fuel-bound sulfur appears to affect the condensable species fraction of the particulate emissions from diesel engines (e.g., H_2SO_4) strongly [1]. Thus, it is not clear that soot particle concentrations are reduced directly as fuel-bound sulfur is reduced.

Regarding your question as to the practical implications of our finding with regard to carbon disulfide addition, we are not proposing the addition of sulfur to fuels to reduce soot. As our study shows, the chemical pathway by which the additive affects the soot formation chemistry is important, whether that is by an alcohol or a sulfur-containing species. As we observed, some alcohol additives increased soot formation. Thus, the key to a reduction in soot formation via a chemical route lies in the formulation of the additive. It is hoped that our work lends insight into that process under diffusion flame conditions.

REFERENCE

1. *Diesel Particulate Emissions: Measurement Techniques, Fuel Effects, Control Technology*, (J. H. Johnson, T. M. Baines, and J. C. Clerc, Eds.), SAE, Inc., Warrendale, PA, 1992.

Attachment B

Spatial and Time Resolved Soot Volume Fraction Measurements in Methanol / Benzene Droplet Flames

by

S. B. Gupta, T. Ni and R. J. Santoro

Eastern States Section of The Combustion Institute,
Fall Technical meeting, 1994.

Spatial and Time Resolved Soot Volume Fraction Measurements in Methanol/Benzene Droplet Flames

S.B. Gupta, T. Ni and R.J. Santoro
Propulsion Engineering Research Center
Department of Mechanical Engineering
The Pennsylvania State University
University Park, PA 16802

Abstract

Planar laser-induced incandescence (2D-LII) was used to measure spatially resolved soot-volume fraction profiles at various points of time during droplet combustion. Using this technique soot volume factions (f_v) up to 38 ppm in flames of methanol (CH_3OH)/benzene (C_6H_6) mixture droplets, with initial diameters in the range 0.6-1.0 mm were measured. Reductions in soot indices up to 90% were observed with 75% addition of methanol by liquid volume. In earlier stages, rapid preferential vaporization of less sooty methanol, and in later stages oxidant entrainment due to increased convection are believed to result in such reductions.

Introduction

Although sooting characteristics of droplet flames have been of interest in many previous studies, they have been severely limited by the lack of proper diagnostic techniques. Kadota and Hiroyasu[1] have used laser extinction-scattering to measure the soot profiles of droplets suspended by quartz fibers in a quiescent atmosphere. Randolph and Law[2] have used a phase-differentiating probe to sample the soot formed around freely-falling droplets for quantitative measurements. However, no measurements have been reported to date characterizing both the temporal and spatial formation of soot in free-falling droplet flames. In this study, Laser-Induced Incandescence (LII), a technique which in the recent past has been identified to be a versatile diagnostic technique in the measurement of soot-volume fraction,[3,4] has been used to study the sooting characteristics of benzene / methanol droplet flames.

Soot reductions due to alcohol addition have been reported in many studies on liquid and gaseous mixture flames.[2,3] Ni et al.,[3] report soot reductions in ethylene flames up to 60% by addition of 14% methanol. The authors claim this reduction to be mainly due to chemical effects. Randolph and Law[2] studied droplet flames of alcohol/aromatic blends. They attribute soot reductions mainly to the volatile nature of alcohols, which introduced a dilution effect. In the present study mixtures of benzene and methanol have been used to further study such effects.

Experimental

Figure. 1 shows the setup used for the 2D-LII imaging. Central to this setup is an aerodynamic droplet generator based on the suggestions by Green et al.,[5] This droplet generator is placed at the center of a flat-flame burner, which in turn is placed at the top of a combustion chamber which has flat quartz windows to provide optical access. Droplets of initial diameters (d_o) between 0.6 and 1.0 mm issuing from the droplet generator are ignited on traversing the flat flame. The CH_4+O_2+Air mixture that passes through the flat-flame burner allows the droplets to burn in an atmosphere of 21% O_2 mole fraction. In such an arrangement, the ambient temperature inside the combustion chamber varied from 670°C at the top to about 360°C at the bottom.

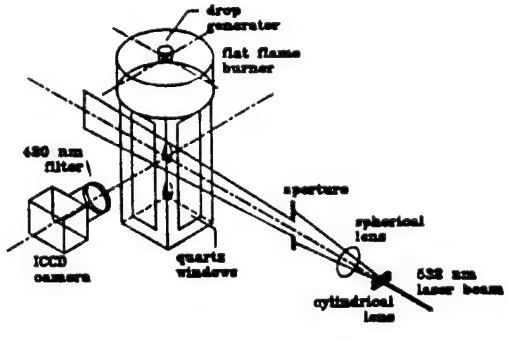

Fig. 1 Experimental setup for 2D-LII imaging

The 532 nm beam from a pulsed Nd:YAG laser is passed through a combination of a 1 m focal length bi-convex lens and a 6 cm focal length cylindrical lens separated by approximately 6 cm. The focus of the vertical laser sheet is aligned to be at the center of the test cell. An aperture placed between the lenses and the test cell is used to obtain a sheet of uniform power density about 3.8 cm in height at the center of the test cell. A CCD camera equipped with a micro-channel plate intensifier, placed at 90° to the laser sheet, is used to capture the images. A 420±5 nm bandpass filter and a

combination of 105 mm Nikon lens attachment and bellows focusing attachment in front of the camera image the soot volume fraction profiles on the CCD array. Further details of this technique are described in the work of Ni et al.[6]

Stroboscopically backlighted images of freely falling droplets recorded on a standard video tape recorder system provided drop-size and velocity information. However, as the test cell was designed to study only the initial portion (less than a 1/5) of the droplet lifetime, the drop-sizes remain virtually unchanged. Hence, the droplet diameters are assumed to be constant throughout this study.

Results and Discussion

The soot histories of droplets of methanol/benzene mixtures, for concentrations of 25% and 75% by liquid volume (i.e., 0.131 and 0.577 mole fraction of benzene) are shown in Fig. 2. When a droplet of these mixtures is ignited, the soot volume fraction (f_v) is observed to initially increase with time followed by a decrease as the droplet burning continues. Peak values of f_v as large as 38 ppm are observed during combustion. The addition of increasing amounts of methanol to the droplet is observed to reduce the amount of soot formed in the droplet wake region at similar residence times.

The structure of the soot particle field in the droplet wake region is similar to that observed in gaseous co-flow laminar diffusion flames.[3] In Fig. 2b (t=43 ms), regions of soot inception, growth and oxidation can easily be identified. The similarity between the soot fields is a result of the fact that both combustion events are characterized by diffusion controlled mixing, which results in a similar flame structure. The temporal variation of the soot evolution for the droplet case is due to a combination of effects related to the burning of fuel mixtures and the variation in convective effects[2]. These effects will be discussed below. Figure. 3a provides a schematic of the structure of the combustion field surrounding the droplet while figures 3b and 3c show results obtained by simultaneous planar imaging of laser-induced fluorescence from OH-radicals and 2D-LII measurements of f_v behind a free-falling combusting droplet. It should be noted that throughout the observation period, the OH radicals envelope the soot containing region.

Effect of Methanol Addition :

As identified by Wang et al.,[7] when a droplet of a binary-mixture is ignited, the volatile component is preferentially vaporized initially. This vaporization is sustained by its supply from a thin surface layer through which diffusion is rapid because of the short characteristic length of traverse. However, as the concentration of the volatile component in this layer is steadily diminished, replenishment from the inner core becomes slow because of the exceedingly slow rate of liquid-phase mass diffusion.[7] As time proceeds, the vaporization rate of the individual components should follow their initial concentrations in the initial mixture. This leads to a soot history dominated by the sooting nature of the volatile fuel during the earlier parts, which is followed by that characteristic of the initial concentration of the binary mixture.[7]

The soot histories of droplets of methanol/benzene mixtures studied here closely follow the description of Wang et al.[7] When a droplet of these mixtures is ignited, methanol is preferentially vaporized initially leading to very little net soot emissions. This is soon followed by the liquid-phase diffusion limited combustion. As volatilities of methanol and benzene are quite close (boiling points being respectively 65°C and 80°C) this diffusion limit is reached quiet early in the burning phase. This explains the soot cloud moving towards the droplet in the first two frames (t = 30, 43 ms) of Fig 2b. In the subsequent frames, we find the soot cloud gradually moves away from the droplet, which can be attributed to increased oxidizer entrainment due to convection.

As identified by Jackson et al.,[8] the azeotropic data of methanol/benzene mixtures could govern their vaporization characteristics. The existence of a negative azeotrope[9] at 57.5°C implies preferential vaporization of benzene for its mixture fractions <58.5% by volume. However, as the gas diffusion coefficient of methanol is greater than that of benzene - estimates being 0.104 cm^2/sec and 0.056 cm^2/sec for CH_3OH/N_2 and C_6H_6/N_2 mixtures respectively - it could be argued that rapid transport and the subsequent depletion of methanol vapors immediate to the droplet surface leads to its greater vaporization.

Effect of Droplet Size:

As identified by Jackson et al,[8] the residence time of fuel molecules in the gas-phase between the droplet surface and the flame increases with diameter (being proportional to d^2 for spherically symmetric quasi-steady droplet combustion). Thus, larger droplets allow more time for fuel molecules to break down and the subsequent formation and nucleation of soot precursors.

The temporal evolution of soot indices,[2] S (mg/drop), with time for different droplet sizes are plotted in Fig. 4. The increase in soot indices with droplet size is quite evident. If a d^n dependence is assumed, n values are found to lie between 3 and 4; the non-linearity of the gas-phase reactions leading to soot growth can be identified to be dominant over other physical mechanisms.

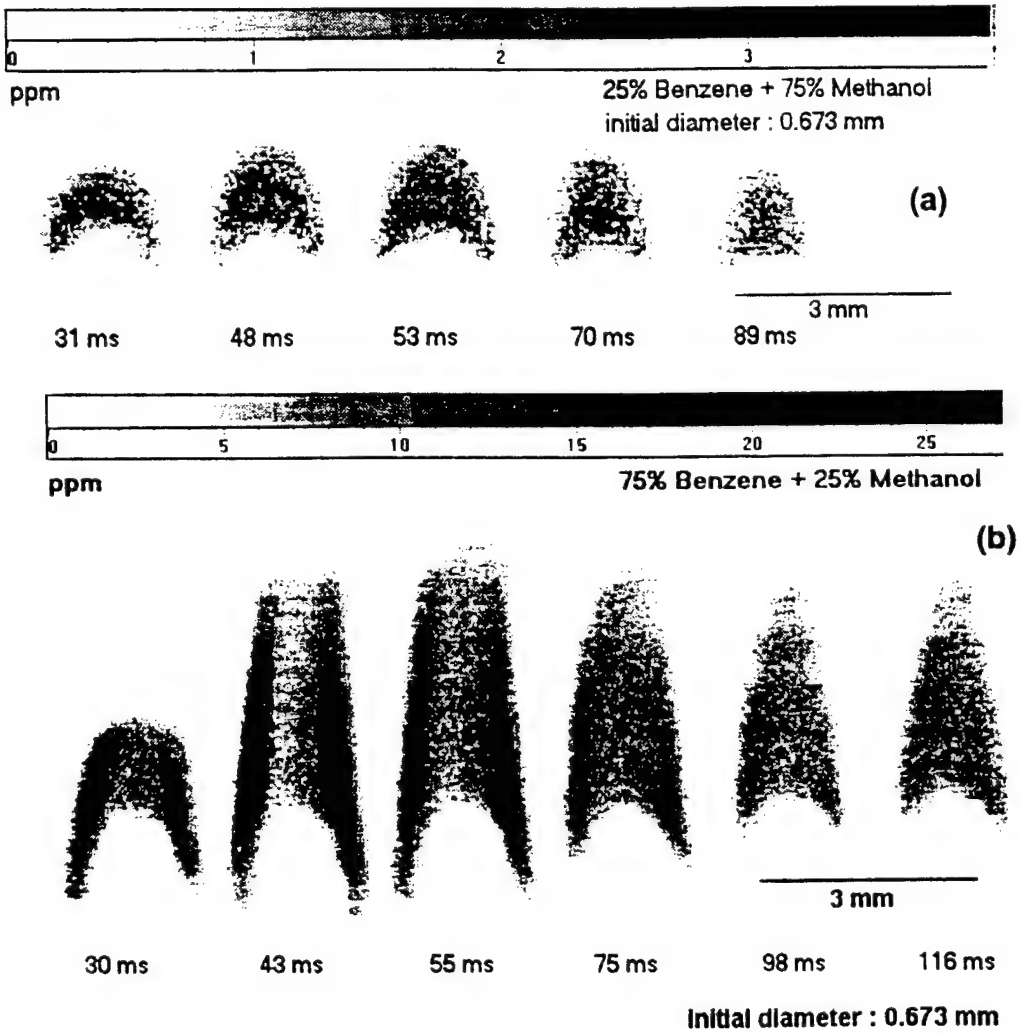

Fig. 2 Time evolution of soot volume fraction profiles in free-falling droplet flames: a) 25% benzene+75% methanol, b) 75% benzene+25% methanol.

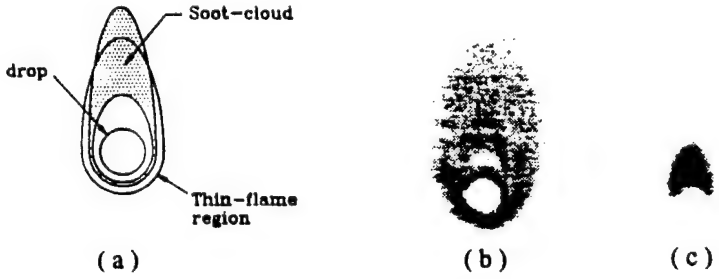

Fig. 3 a) Schematic explaining soot development during convective droplet combustion, b) OH-Fluorescence profile in a droplet flame, c) corresponding soot volume fraction profile (obtained by LII).

Summary and Conclusions

Based on the present state of understanding, the phenomenology of soot formation around a moving droplet can be depicted as described in the work of Law and co-workers[2,7] :

In the early part of its lifetime, the droplet undergoes thermal heating from the surroundings, during which fuel vaporization is relatively negligible. Later, due to vaporization of the fuel and its subsequent pyrolysis a flame front exists around the drop (cf Fig. 3a). Within this shell, large hydrocarbon molecules formed due to fuel pyrolysis move towards the droplet due to thermophoresis. In this fuel rich region, they undergo growth through coalescence with each other and due to reactions with outwardly diffusing fuel species. These incipient soot particles move away from the droplet and towards the flame front due to convection. As the soot particles traverse the flame front, aided by the increased oxygen availability and higher temperatures they undergo rapid oxidation. Soot particles which survive this oxidation process constitute the net soot emissions from the droplet flame. As velocity of the droplet increases in time, the incipient soot particles aided by buoyancy and convection are transported to the rear of the droplet where they undergo oxidation. At increased convection combustion occurs in the wake region, which being premixed to a certain extent leads to less sooty emissions.

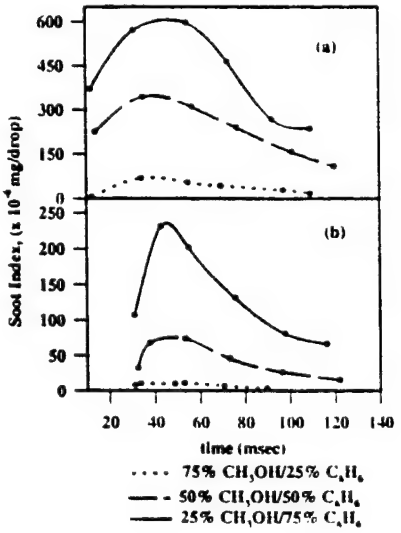

From observations made in this study, the following conclusions can be listed:

1) 2D-LII has been used to measure temporal and spatial soot-volume fraction profiles in flames of freely falling droplets. Using this technique f_v up to 38 ppm have been measured in droplet flames of methanol and benzene blends. Soot indices calculated assuming concentric flame structure are of the same order as those reported previously.[2]

2) The soot profiles around burning droplets have a structure similar to laminar diffusion flames.

3) Results indicate substantial reductions in the instantaneous soot around droplets due to methanol addition. This can be attributed to the preferential vaporization of methanol over benzene in the initial parts of the droplet lifetime and possibly to oxidizer entrainment due to increased convection in the latter parts.

4) Convective transport is found to strongly affect the net soot emissions from the droplet.

Though many physical mechanisms could be identified to affect the soot formation in methanol/benzene droplets, chemical action by methanol could not be unambiguously ascertained.

Fig. 4 Soot histories of free-falling droplet flames;
(a) $d_o \approx 1.0$ mm (b) $d_o \approx 0.67$ mm

References

1. Kadota, T. and Hiroyasu, H., *Combustion and Flame* 55: 195-201 (1984).
2. Randolph, A. M. and Law, C. K., *Combustion and Flame* 64: 267-284 (1986).
3. Ni, T., Gupta, S. B. and Santoro, R. J., *Twenty-Fifth Symposium (International) on Combustion,* The Combustion Institute, Pittsburgh, in press.
4. Quay, B., Lee, T-W., Ni, T. and Santoro, R. J., *Combustion and Flame*, 97:384-392 (1994).
5. Green, G. J., Takahashi, F., Walsh, D. E. and Dryer, F. L., Eastern States Section/ Combustion institute meeting (1988)
6. Ni, T., Pinson, J. A., Gupta, S. B. and Santoro, R. J., *"Two-Dimensional Measurements of Soot Volume Fraction Using Laser Induced Incandescence,"* submitted to Applied Optics.
7. Wang, C. H., Liu, X. Q. and Law, C. K., *Combustion Flame* 56: 175-197 (1984)
8. Jackson, G. S., Avedesian, C. T. and Yang, J. C., *Proceedings of Royal Society of London* 435, pp 359-369 (1991)
9. Horsley, L. H., and co-workers, "*Azeotropic Data - III*," Advances in Chemistry Series(1963)

Attachment C

Two-dimensional Imaging of Soot-volume Fraction Using Laser-induced Incandescence

by

T. Ni, J. A. Pinson, S. B. Gupta, and R. J. Santoro

Applied Optics, Vol. 34, No.30,
Oct. 1995, pp. 7083 - 7091.

a reprint from Applied Optics

Two-dimensional imaging of soot volume fraction by the use of laser-induced incandescence

T. Ni, J. A. Pinson, S. Gupta, and R. J. Santoro

A recently developed laser-induced incandescence technique is used to make novel planar measurements of soot volume fraction within turbulent diffusion flames and droplet flames. The two-dimensional imaging technique is developed and assessed by systematic experiments in a coannular laminar diffusion flame, in which the soot characteristics have been well established. With a single point calibration procedure, agreement to within 10% was found between the values of soot volume fraction measured by this technique and those determined by conventional laser scattering–extinction methods in the flame. As a demonstration of the wide range of applicability of the technique, soot volume fraction images are also obtained from both turbulent ethene diffusion flames and from a freely falling droplet flame that burns the mixture of 75% benzene and 25% methanol. For the turbulent diffusion flames, approximately an 80% reduction in soot volume fraction was found when the Reynolds number of the fuel jet increased from 4000 to 8000. In the droplet flame case, the distribution of soot field was found to be similar to that observed in coannular laminar diffusion flames.

Key words: Laser-induced incandescence, soot, flames.

1. Introduction

Recently the effectiveness of laser-induced incandescence (LII) for the quantitative determination of local soot volume fraction in laminar diffusion flames[1,2] was demonstrated. Because this diagnostic technique provides a direct measure of soot volume fraction without the need for a tomographic inversion process, as is used in conventional line-of-sight laser extinction methods, it was suggested that LII could be applied for instantaneous planar measurements of soot volume fraction in combustion systems, including nonsymmetric or unsteady flames. The applications of LII in qualitative two-dimensional (2-D) soot field imaging of diffusion flame and diesel engine combustion have been previously reported.[3–5] With the use of a calibration scheme described in the earlier work for point measurements,[1] it is possible to obtain quantitative 2-D imaging of soot volume fraction.

LII arises from near-blackbody emissions that originate from laser-heated soot particles. Theoretical analysis has shown that when the laser pulse is sufficiently intense, LII emission in the visible wavelength range is approximately proportional to local soot volume fraction.[6] This prediction has been verified experimentally in the previous work involving point measurements in an ethene–air laminar diffusion flame.[1] Recent work that address premixed flat flames have observed similar results and have examined the effects of interfering radiation such as background flame luminosity and fluorescence from polycyclic aromatic hydrocarbons[7] (PAH's). Studies in which LII is used to measure soot volume fraction in flickering ethene–air diffusion flames have also been reported.[8]

In this paper, we address key issues associated with quantitative measurements made by using 2-D LII imaging and describe the novel application of 2-D LII in the measurement of soot volume fraction in laminar diffusion, turbulent diffusion, and free-falling droplet flames. To gain better understanding of the behavior of the LII technique and to provide information for the design of experiments by the use of 2-D

The authors are with the Department of Mechanical Engineering and the Propulsion Engineering Research Center, The Pennsylvania State University, University Park, Pennsylvania 16802-2320.

Received 29 August 1994; revised manuscript received 11 May 1995.

0003-6935/95/307083-09$06.00/0.

LII imaging, we also made a number of point measurements.

2. Experimental Approach

A. Experimental Apparatus For Point Measurements

The optical setup for the point measurements utilizes a frequency-doubled Nd:YAG pulsed laser (Surelite II, Continuum) operating at 10 Hz with a pulse width of 7 ns FWHM. For studying the effects of the laser beam intensity profile on the LII signal, two types of intensity profiles were used. These are referred to as the near-Gaussian profile and the rectangular profile hereafter, and they indicate the shape of the intensity profile across the laser beam. The rectangular-profile beam, i.e., one in which the laser intensity is uniform across the beam, was produced when a 1-mm-diameter pinhole was placed in front of the flame, which allowed only the center portion of a 6-mm-diameter near-Gaussian laser beam to heat the soot particles. Because the 1-mm-diameter pinhole is only 6 cm away from the flame, the diffraction effects from the pinhole are negligible. The intensity of the laser beam was varied by the use of a combination of a half-wave plate and a polarization beam splitter. The LII signal at a 90° angle was focused onto the entrance slit of a 0.25-m monochrometer (Instruments SA H20) and was detected by a photomultiplier tube (PMT) (Hammamatsu R928) wired for fast response. The combination of a 0.25-mm entrance slit width for the monochrometer and the 1-mm beam diameter of the laser defined the probe volume for the point measurements. A narrow-band interference filter (10 nm FWHM, transmittance peaks at 400 nm) was placed in the front of the monochrometer in order to reject scattered laser light. The output from the PMT was input to a 100-MHz digital oscilloscope (Tektronix TSA 2440) and then transferred to a lab computer by a general-purpose interface bus. A coannular laminar diffusion flame that burns ethene in air was used in this study. The burner that was identical to the one used in previous soot studies[9,10] consists of a 1.1-cm-diameter fuel tube surrounded by a 10.2-cm-diameter air tube. The flow rates of ethene and air were 3.85 cm^3/s and 1060 cm^3/s, respectively. At this flow condition, the distribution of soot volume fraction and soot particle size have been measured by a light scattering–extinction method.[9]

B. Experimental Apparatus For Two-Dimensional Laser-Induced Incandescence Imaging

The experimental setup for 2-D LII imaging is shown in Fig. 1. A 285-mJ/pulse, 532-nm laser beam (Gaussian profile at far field) from the YAG laser was shaped into a 350-μm-thick (FWHM) laser sheet by a combination of a diverging cylindrical lens [focal length (fl) = 6 cm] and a spherical focusing lens (fl = 2 m). The thickness of the laser sheet was measured by translation of a razor blade across the laser sheet and measuring the transmitted energy. For quantitative 2-D LII measurements, the uniformity of the laser sheet is particularly important. A good laser sheet was obtained when the diverging cylindrical lens was placed close the laser exit, as the laser beam profile at near field is nearly flat. Although the laser sheet at the focal point was ~32 cm in height, only the central 10 cm were used for 2-D LII imaging to ensure the uniformity of the laser sheet. The uniformity of the center 10 cm of the laser sheet was better than 90% as determined when a 2-mm-wide slit was moved vertically along the laser sheet and the transmitted laser power was measured. The use of a very long fl lens (fl = 2 m) has the advantage of minimizing the variation of the thickness of the laser sheet across a flame, which is especially important when large-diameter flames are being studied. For an imaging area as wide as 5 cm, the variation of the thickness is estimated to be less than 5%. Furthermore, the sensitivity of LII imaging is higher when a longer fl lens is used, as the LII signal is directly proportional to the thickness of the laser sheet, which is larger for a longer fl lens. For large-diameter flames, the use of a thicker sheet is particularly important, as it helps in rejecting background luminosity, which is nearly proportional to the diameter of the flame.

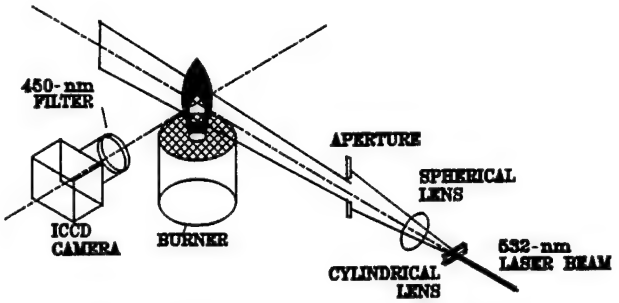

Fig. 1. Experimental setup for 2-D LII imaging.

The LII images were taken at a 90° angle to the laser sheet by a gateable intensified CCD camera (Princeton Instruments, Model ICCD-576S/RB) equipped with a 105-mm fl UV camera lens (Nikkon, $f/4.5$). The spatial resolution for these 2-D imaging studies is determined by the number of camera pixels (578 × 384) available and the field of view imaged in the experiments. The resolutions for each of the studies described here are included in the appropriate sections below. A broadband interference filter (450 ± 25 nm) was placed in front of the camera to minimize the interference from scattered light. A small amount of scattered light was found to pass through the filter. The influence of the scattered light was completely eliminated when the intensifier was gated on after the laser pulse. Although a stronger signal could be obtained if a long gate time were employed, the gate time for the intensifier in this experiment was set at 18 ns, which is much shorter than LII decay time, to minimize the effect of particle size, which is discussed below.

The interference from fluorescence of PAH's has been examined. For ethene coflow diffusion flames,

PAH's are mostly present at lower flame heights and at radial locations that are closer to the center line compared with soot particles.[2] In these PAH formation regions where soot particles are absent, no significant signal was observed in the LII imaging experiments, indicating that fluorescence from PAH does not interfere with the LII signal. This may be due to the observation that PAH species emit predominantly at wavelengths longer than the excitation wavelength (532 nm), whereas the LII signal was captured at a shorter wavelength (450 nm). To prevent flame luminosity from leaking through the intensifier when the gate is off, a mechanical shutter that opens for 5 ms during image acquisition was placed in front of the camera lens. With a modest intensifier gain, the single-shot signal from 10 parts in 10^6 (ppm) soot in an ethene diffusion flame is ~3000 counts/pixel for a probe volume of 170 μm × 170 μm × 350 μm. The sensitivity can be enhanced by increasing the bandwidth of the interference filter. In the present imaging experiment, the camera was gated on immediately after the laser pulse. When the slightly delayed LII signal was measured, the intensity of the acquired images was found to remain nearly constant for an average laser fluence beyond 0.17 J/cm^2. Measurements were taken at a laser fluence of 0.32 J/cm^2 or an intensity density of 4.6×10^7 W/cm^2. This laser fluence is approximately a factor of 8 lower than that used in our previous work for point measurements.[1] The use of low laser fluence has the advantage of minimizing intrusion of the LII process on the flame that is due to laser vaporization of soot particles and thus has potential for applications in systems in which successive images are needed.

After dark noise was subtracted, the LII images were corrected for the combined spatial variations in CCD pixel response and intensifier gain when the ratio of the LII image to a correction image was taken. The correction image was obtained by the uniform illumination of the camera by a lamp located behind a diffusor. The corrected LII images were then translated into soot volume fraction images after the imaging system was calibrated against a sooting source whose soot volume fraction is known. In this experiment, an ethene diffusion flame served as the calibration standard.[1] The LII images were not corrected for the absorption of LII signal by soot particles located between the laser sheet and the camera. Although using longer detection wavelengths could reduce the extinction of the signal, the background luminosity becomes more difficult to reject.

3. Laser-Induced Incandescence Signal Characteristics

A. Laser Fluence Effects

The intensity of a LII signal depends on the temperature of the laser-heated soot particles, which is determined by the rate of laser energy absorption and heat loss through conduction, radiation, and soot vaporization. It has been observed[1] that initially the LII signal increases rapidly as laser fluence increases. Once laser fluence reaches a saturation threshold the LII signal shows a small or no increase with respect to an increase in laser fluence. At high laser fluence it is believed that soot vaporization is the dominant effect that limits the increase in soot particle temperature. Using a laser fluence in the saturation regime is desirable when one is measuring soot volume fraction, as the LII signal is then least affected by laser beam attenuation across the flame. However, there is a significant uncertainty in measuring the local laser fluence in an ordinary laser beam, which is not uniform. It is therefore difficult to determine the saturation intensity accurately under many conditions. In order to study the effect of laser fluence on the LII signal, a rectangular-profile laser beam was used to heat the soot particles. Theoretical models[11,12] for particle heating and vaporization have been reported previously as a function of laser fluence. The use of the rectangular-profile beam allows the laser fluence to be easily determined, thereby allowing direct comparison with theory.

Figure 2 illustrates the effect of laser fluence on the intensity of the LII signal detected immediately after the rectangular-profile laser pulse. These results were obtained in an ethene laminar diffusion flame at a height 40 mm above the fuel tube exit and at a radial location where peak soot volume fraction is observed for this height. Below a laser fluence threshold of 0.06 J/cm^2, no observable LII signal was detected. Just above the laser fluence threshold, the LII signal exhibits a rapid increase with increased laser fluence. After the LII signal reaches a peak at a laser fluence of 0.27 J/cm^2, further increase of laser fluence actually reduces the LII signal intensity. Similar results have been observed recently by Vander Wal and Weiland[13], who used a Gaussian-profile laser beam. A profile that exhibits a rapid increase in the

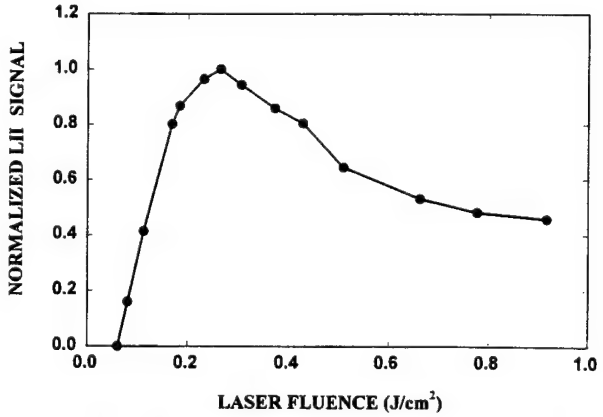

Fig. 2. Effect of laser fluence on LII for a rectangular laser intensity profile (rectangular profile). These measurements correspond to an ethene–air laminar diffusion flame at an axial position 40 mm above the fuel tube exit and a radial location exhibiting the peak soot volume fraction for that height.

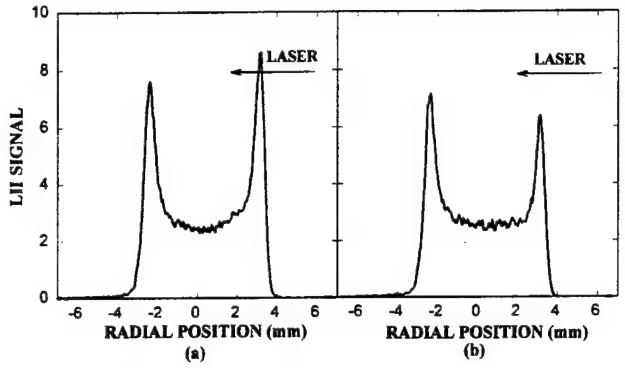

Fig. 3. Effect of laser fluence on the spatially resolved LII signal profile at a height 40 mm above the fuel exit of an ethene–air laminar diffusion flame: (a) laser fluence 0.15 J/cm^2, (b) laser fluence 0.41 J/cm^2.

LII signal followed by a slow decrease as a function of laser fluence has been predicted by Tait and Greenhalgh[3] from numerical calculations. They predicted that a decrease in particle mean volume that is due to vaporization at high laser fluence reduces the LII signal intensity. The spatially resolved LII signal profiles across an axisymmetric ethene diffusion flame at the 40-mm height are shown in Fig. 3. Because of the extinction of the laser beam by soot particles, which results in a 20%–25% reduction in the laser intensity across the flame, the LII profiles are asymmetric. For a laser fluence below saturation, the LII signal from the peak that is closer to the laser source is stronger [shown in Fig. 3(a)], as the effect of laser attenuation dominates over soot vaporization. In contrast, for a laser fluence beyond the saturation fluence, the signal from the far peak is stronger [shown in Fig. 3(b)], as soot vaporization is now the dominant perturbation that affects the LII signal.

A temporal profile of the vertically polarized light-scattering signal and the influence of laser intensity on the temporal profile of the LII signal are shown in Fig. 4. For a laser intensity slightly above the threshold, the LII signal rises slowly and reaches its maximum just after the laser pulse, which indicates that the temperature of the soot particles is constantly increasing during the laser pulse. As laser fluence increases, the rise time and the decay time of the LII signal decrease, while the maximum in the LII signal is observed to increase at lower laser fluence (<0.27 J/cm^2) and decrease at higher laser fluence (>0.27 J/cm^2). The initial increase in the maximum of the LII signal and the decrease of the LII signal rise time with increased laser fluence are consistent with the observation that soot particles are heated to a higher temperature and that the temperature rises faster at a higher laser intensity.[11] The dramatic decrease of the LII decay time with increased laser fluence, as shown in Fig. 5, is not fully understood. One explanation is that the vaporization of soot particles under intense laser heating reduces their size, and the smaller particles consequently cool faster. Dasch[12] showed that vaporization reduces the diameter of soot particles, D, exponentially with laser fluence, F, as

$$D = D_0 \exp[-(F - F^*)/F_0], \quad (1)$$

where D_0 is the initial particle diameter and F^* and F_0 are empirical parameters that can be determined experimentally. For a 7-ns laser pulse, the threshold fluence F^* and decay fluence F_0 have been reported to be 0.23 J/cm^2 and 1.9 J/cm^2, respectively.[12]

For a laser fluence of 0.54 J/cm^2, the calculated reduction in soot particle size from Eq. (1) is 15%. Under the same laser fluence, the LII decay time is approximately a factor of 10 times shorter than the decay time under a laser fluence of 0.11 J/cm^2. Such a significant decrease in the decay time cannot be explained by the vaporization mechanism alone. It is likely that, in addition to the vaporization mechanism, other physical or chemical properties of the soot particles change under the intense laser fluences involved in the particle-heating process. Dasch[12] measured light scattering and absorption of a

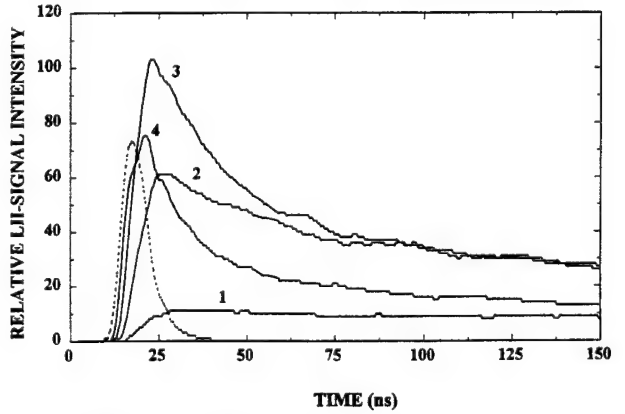

Fig. 4. Effect of laser fluence on the temporal profile of the LII signal: dashed curve, laser scattering signal; trace 1, laser fluence 0.072 J/cm^2; trace 2, laser fluence 0.14 J/cm^2; trace 3, laser fluence 0.27 J/cm^2; trace 4, laser fluence 0.72 J/cm^2.

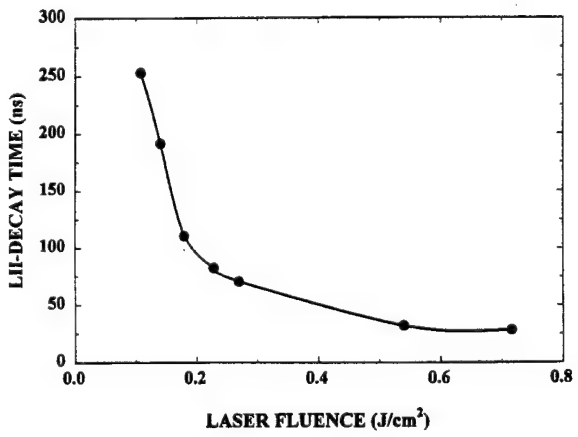

Fig. 5. Effect of laser fluence on the LII signal decay time (the time for the signal to decay to $1/e$ of peak intensity).

cw probe laser along a high-energy pulsed laser beam and concluded that soot particles vaporize rather than fragment. However, by a careful examination of the time-resolved light-scattering signal obtained by Dasch,[12] it can be found that there is a transient, but significant, reduction in light scattering during or immediately after the laser pulse, which Dasch attributed to scattered light from the laser pulse or induced incandescence. This transient signal could also be interpreted as indicating that soot aggregates undergo a rapid change in shape, resulting in an increased surface area and a faster heat loss.

From these results, it is clear that at the laser fluences required for LII measurements, significant effects on the LII signal decay time can be observed as the laser fluence is varied. Thus the observed response of LII signal intensity to the laser fluence is sensitive to the delay time for detector gate pulse with respect to the laser pulse. The LII signal during the initial laser-heating period is particularly sensitive to the laser fluence. For quantitative soot volume fraction measurements, the detector gate should be delayed by few nanoseconds with respect to the laser pulse.

B. Particle-Size Effects

Figure 6 shows the temporal profiles of a LII signal obtained in the ethene–air laminar diffusion flame at heights of 10 and 30 mm above the fuel tube exit and at the radial locations corresponding to peak soot volume fraction for these heights. These observations were made with the rectangular-profile laser beam with a laser fluence of 0.27 J/cm^2. Spatially resolved particle-size measurements on this flame have been performed by Santoro *et al.*[9] The mean particle diameter (D_{63}) of soot particles at the 30-mm height is 160 nm, which is significantly larger than that observed at the 10-mm height, where the mean size is 64 nm. As can be seen in Fig. 6, the leading edges of LII temporal profiles at the two locations in the flame closely match, which is consistent with the theoretical prediction,[3] indicating that in the Rayleigh regime all particles, regardless of size, increase in temperature at the same rate. In contrast, the LII signal at the 10-mm flame height undergoes a faster decay than that observed at the 30-mm height. This behavior is due to the difference of the soot particle size, as smaller particles have a larger surface area per unit mass and are expected to cool faster.

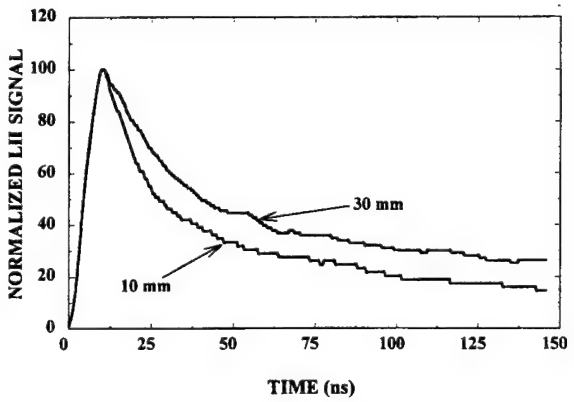

Fig. 6. Temporal profile of a LII signal obtained in the ethene–air laminar diffusion flame at heights of 10 and 30 mm above the fuel tube exit and at the radial locations corresponding to peak soot volume fraction for these heights.

To demonstrate this particle-size effect and estimate the error associated with the detection delay time, a one-dimensional (1-D) LII imaging experiment was performed. The LII signal generated by the rectangular-profile laser beam was imaged onto the gated intensified CCD camera. A narrow-band interference filter with transmittance centered at 400 nm was placed in the front of the camera to reject scattered laser light and PAH fluorescence. The camera was gated on for 5 ns. Figure 7(a) shows the normalized 1-D LII signal profiles from the ethene–air laminar diffusion flame at the 40 mm height, obtained by the varying of the delay time of the intensifier gate with respect to the laser pulse. Figure 7(a) contrasts the results obtained when the gate is placed immediately after the laser pulse compared with the case in which the gate is delayed 180 ns. It can be seen that the LII signal ratio of center line to the peaks decreases as the intensifier

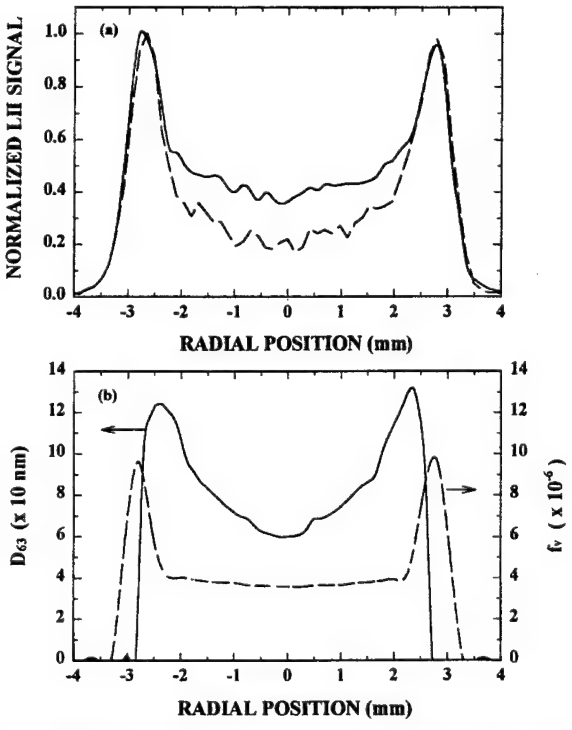

Fig. 7. Effect of the delay time of the detector gate on the spatial profile of the LII signal at the 40-mm height in the ethene–air laminar diffusion flame: (a) solid curve, LII signal observed immediately after laser pulse; dashed curve, LII signal observed 180 ns after the laser pulse; (b) laser scattering–extinction data,[9] where the solid curve is the soot mean particle diameter, and the dashed curve is the soot volume fraction.

gate pulse was delayed for 180 ns with respect to the laser pulse. This observation is consistent with the particle-size measurements at that height, which are shown in Fig. 7(b). Compared with soot volume fraction data at the same flame height [shown in Fig. 7(b)] measured by the laser scattering–extinction method,[9] the LII profile taken immediately after the laser pulse matches closely with the laser scattering–extinction data. Similar results were also observed for the Gaussian-profile laser beam. Because of this size dependence, the delay time between laser pulse and detector gate for an imaging experiment should be made as short as possible to minimize this particle-size effect. Even though the LII signal can last as long as 600 ns, a short detector gate width should be used so that the contribution from the size-sensitive portion of LII signal is minimized. For a gate width of 50 ns, the error that is due to the size effect could be as large as 10%, as estimated by the integration of the LII signals, shown in Fig. 6, over the time period of the gate width.

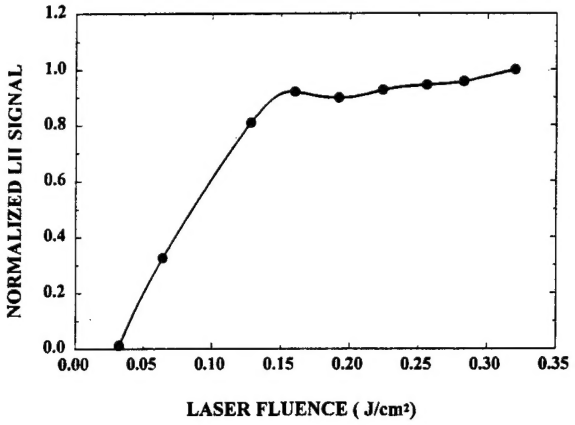

Fig. 8. Effect of average laser fluence on LII for a Gaussian-shaped laser beam. These measurements correspond to an ethene–air laminar diffusion flame at an axial position 40 mm above the fuel tube exit and a radial location that exhibits the peak soot volume fraction for that height.

C. Laser Beam Shape Effects

The results describe above were obtained with the use of a laser pulse whose spatial profile is rectangular compared with a Gaussian beam. However, typically lasers do not generate a rectangular-profile beam. Although the use of a pinhole can reshape the Gaussian beam into a rectangular-profile beam, the spatial resolution is relatively low because of the diffraction effect from the pinhole. The use of a pinhole also reduces the efficiency of laser power utilization. Thus it is not feasible to use a rectangular-profile beam in a 2-D LII imaging measurement that requires very high laser energies to form a laser sheet intense enough to saturate the LII signal.

For a near-Gaussian-profile beam, the laser intensity is not uniformly distributed. Increasing laser energy will result in an increase in the effective LII probe volume, in which the local laser fluence exceeds the threshold for the LII signal to be observed. Figure 8 shows a plot of the LII signal taken immediately after the laser pulse as a function of average laser fluence of the laser sheet. The LII signal was obtained in the ethene–air laminar diffusion flame at a height of 40 mm above the fuel tube exit and at the radial location that corresponds to peak soot volume fraction for this height. The intensified CCD detector was gated on for 18 ns. The laser intensity across the laser sheet has a near-Gaussian profile. The thickness of the laser sheet is $\sim 350\ \mu m$ (FWHM). The LII signal intensity shown in Fig. 8 is seen to be nearly constant for a laser fluence beyond $0.17\ J/cm^2$. This behavior is different from that observed for the rectangular-profile beam, in which the LII signal intensity decreases after saturation.

Previous point measurements[1] in which a near-Gaussian-profile beam was used have shown that for a sufficiently intense laser fluence the LII signal exhibits a small increase with an increase in laser fluence. A similar result was found by Tait and Greenhalgh,[3] who used a laser sheet. It was suggested that, as laser energy increases, the decrease in the LII signal that is due to vaporization of the soot particles was compensated for by an increase in the effective probe volume, resulting in a near-constant LII signal intensity. We have tried to generate LII signals by using a doughnut-shaped beam. However, the LII signal intensity observed continued to increase with higher laser fluence, suggesting that the response of the LII signal to average laser fluence is sensitive to the laser beam intensity profile. This result is likely due to differences in the expansion of the probe volume with respect to the degree of soot particle vaporization.

The interactions between laser beam and soot particles may also have significant effects on the beam profile. For a Gaussian beam, more soot content is vaporized in the center of the beam than in the outer portion, because the laser intensity in the center of near-Gaussian-profile beam is larger. The vaporization effect decreases the absorption of laser energy by soot particles, particularly in the center of the laser beam. Consequently, as the laser beam propagates through the soot field, the beam diameter becomes smaller, because the wings are preferentially absorbed. The vaporization of soot particles also affects the temporal profile of the laser pulse as the laser beam propagates through the soot field. This effect is due to the fact that the soot volume fraction in the laser beam decreases gradually during the laser pulse, the less energy in the later part of the laser pulse is absorbed. The change in the temporal profile of the laser pulse may affect the response of the LII signal to laser fluence. To minimize the experimental error caused by these effects, the laser fluence should be kept as low as possible. For these reasons, it is not recommended that the technique be used in large-diameter and heavily sooting flames unless care has

been exercised to examine the interaction between the laser beam and the soot particle field.

4. Imaging Results and Discussion

In order to examine and demonstrate various aspects of 2-D LII imaging for soot volume fraction measurements, a series of experiments were conducted that involved an ethene–air laminar diffusion flame, a turbulent ethene diffusion flame and a benzene–methanol droplet flame. These experiments were selected to demonstrate

(1) the comparative accuracy of the 2-D LII technique compared with previous laser scattering–extinction measurements in laminar diffusion flames;
(2) the capabilities of the 2-D LII technique in gaseous, unsteady turbulent diffusion flames;
(3) that 2-D LII imaging can be implemented in the presence of a liquid fuel droplet that introduces additional light-scattering interferences.

A. Laminar Diffusion Flame Measurements

The soot volume fraction image for an ethene–air laminar diffusion flame measured with the 2-D LII imaging technique is shown in Fig. 9. Because soot particle size and concentration information throughout the ethene diffusion flame has been determined,[9,10] it is possible to use this flame for the examination of the accuracy of the 2-D imaging technique.

To provide access for the laser sheet, the brass chimney for the burner used in previous work[9,10] was replaced with a glass chimney. Part of the glass chimney was painted black to minimize the reflection of LII from the chimney wall onto the detector. The flow conditions for the burner were duplicated from previous work.[9] The laser sheet was directed to pass through the center line of the flame. The flame has a visible flame height of 88 mm and does not emit smoke from the flame tip. Thus the 10-cm-wide laser sheet is large enough to cover the entire soot field in the flame. The spatial resolution for the LII images is 170 μm × 170 μm × 350 μm.

To obtain the soot volume fraction image, the observed LII image was scaled so that the LII signal from a pixel corresponding to the radial location where the peak soot volume fraction occurs at the 40-mm height is equal to the soot volume fraction at this location from laser scattering–extinction measurements. A comparison between the soot volume fraction measured by LII imaging and the laser scattering–extinction method for three heights in the flame is shown in Fig. 10. It can be seen that the data measured by the LII technique agrees very well with that obtained by the laser extinction–scattering method.[9] The small different (~5%–10%) between LII data and laser scattering–extinction data is probably due to the effect of particle size. As can be seen, the deviation usually occurs at lower heights or along the flame center line where soot particles are smaller. Numerical analysis performed by Melton[6] shows that the intensity of LII signal at the maximum temperature is proportional to the mean particle diameter raised to the power of $(3 + 0.154\lambda_{det}^{-1})$, where λ_{det} is the detection wavelength in micrometers. For λ_{det} = 450 nm, the exponent is 3.34. The deviation of the exponent from 3 could result in an underestimation of the soot volume fraction for smaller particles if the detection system is calibrated against larger particles. The mean soot particle diameter (D_{63}) in the ethene flame has been measured by Santoro *et al.*[9] to range from 15 to 160 nm. However, the difference between the LII data and the laser scattering–extinction data is significantly smaller than the theoretical prediction.

B. Turbulent Diffusion Flame Measurements

The turbulent diffusion flames were established by the injection of ethene into still air through a 1-mm-diameter 250-mm-long stainless steel tube mounted on a traversing stage. The flow rate of ethene was metered by a rotameter. The 2-D LII measurements were made for two different burner Reynolds numbers (4000 and 8000). The visible flame heights for Re = 4000 and Re = 8000 flames are ~300 mm.

The quantitative single-shot images for soot volume fraction distribution were taken when the 10-cm-wide laser sheet was passed through the center line of the turbulent flames, resulting in a spatial resolution identical to the laminar flame case discussed above.

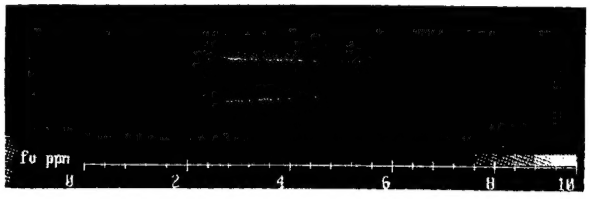

Fig. 9. Soot volume fraction (f_v) image of an ethene–air laminar diffusion flame. The maximum soot volume fraction in the image is 9.8×10^{-6}.

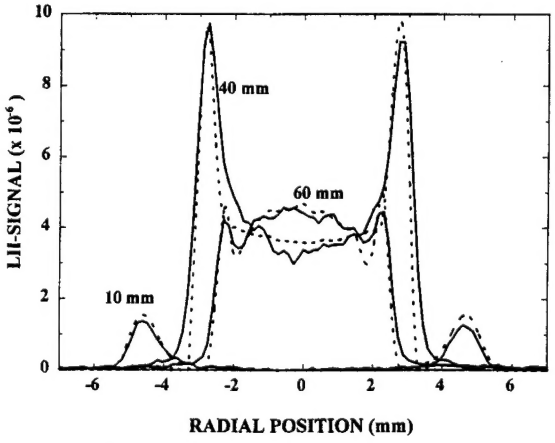

Fig. 10. Comparison of the soot volume fraction profiles obtained by LII and laser scattering–extinction.[9] Solid curve, LII data; dashed curve, laser scattering–extinction data.

The error involving the contribution from background luminosity to the signal intensity in the flames was found to be less than 2%. However, it must noted that the extinction of the LII signal by soot particles located between the laser sheet and the detector may reduce the signal intensity by as much as 10%. Typical soot volume fraction images, extending over the region from 10 to 20 cm above the fuel tube exit, are shown in Fig. 11. The LII images, which show soot particles being confined in turbulent eddies, reveal that the soot distribution is highly intermittent. This soot field structure is similar to the observations made by light-scattering studies for turbulent acetylene[14,15] and natural gas[16] flames. Figure 11 also shows that the soot volume fractions in the Re = 8000 flame are generally lower than those in the Re = 4000 flame by at least a factor of 5. It is believed that the higher Reynolds number associated with higher flow velocity enhances the fuel–air mixing, thereby reducing the time for soot growth. A similar fuel velocity effect on soot formation was reported in the study of turbulent acetylene flames by Kent and Bastin.[17]

C. Free-Falling Droplet Flame Measurements

Single benzene–methanol droplets generated from an aerodynamic droplet generator were injected downward into the postcombustion gas of a flat premixed flame burning methane. The temperature of the postcombustion gas, which contains 21% oxygen, is ~670 °C. To increase spatial resolution for LII imaging in the droplet flame, the 2-m spherical lens was replaced with a 1-m lens to shape the laser beam into a 200-μm-thick sheet. A close-up bellows was placed between the intensified CCD camera and the 105-mm camera lens to increase the magnification of the LII images. For these conditions, the spatial resolution is 30 μm × 30 μm × 200 μm.

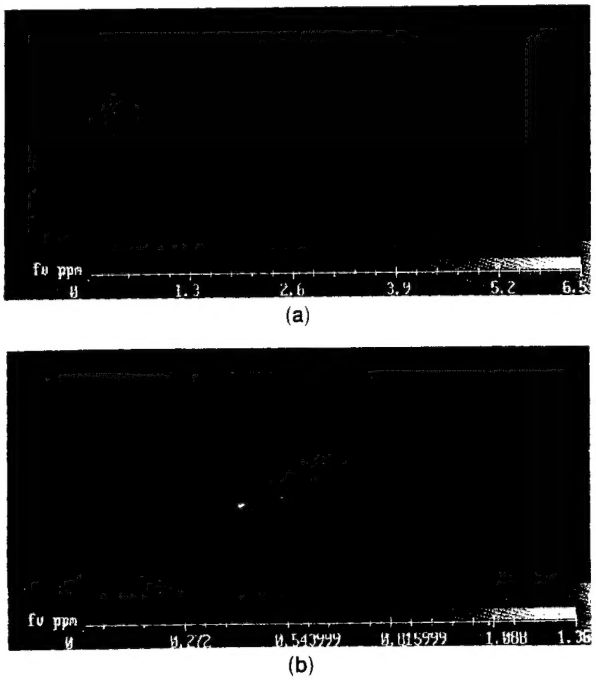

Fig. 11. Soot volume fraction (f_v) images of turbulent ethene diffusion flames: (a) Reynolds number 4000, (b) Reynolds number 8000.

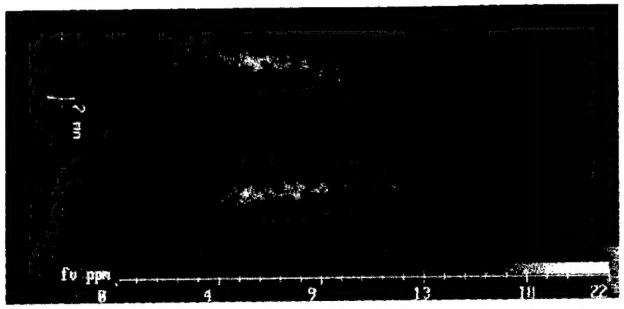

Fig. 12. Soot volume fraction (f_v) image of a freely falling droplet flame.

Figure 12 shows the distribution of soot formed from a 680-μm-diameter burning droplet that contains 75 volume % benzene and 25 volume % methanol. The image was taken 50 ms after the droplet was injected into the postflame gas. Similar to the structure of coannular laminar diffusion flames, the maximum soot volume fractions in this droplet flame are found in an annular region, not along the center line. Because benzene (bp 80 °C) and methanol (bp 65 °C) are highly volatile, the gaseous fuel vaporized from the droplet is concentrated in the wake region behind the droplet, forming a diffusion flame similar to the coannular gaseous flame geometry. The higher soot volume fractions observed in the droplet flame compared with the ethene–air laminar diffusion flame is consistent with the higher sooting tendency of benzene. The soot volume fraction observed in the droplet flame is sensitive to droplet size and methanol concentration. Significant reductions in soot volume fraction were observed by a decrease in the droplet size or an increase in the concentration of methanol.

5. Conclusions

The present investigation extends our previous work on measurements of soot volume fraction by the use of LII. The results of this investigation indicate the following:

(1) The application of LII for instantaneous, quantitative 2-D measurement of soot volume fraction was confirmed by this investigation. There is good agreement between the LII results and laser scattering–extinction data, although the soot volume fractions measured by LII are a little lower in the regions where the mean soot particle diameter is small.

(2) Time-resolved measurements show that the decay time of the LII signal is as long as several hundred nanoseconds and is sensitive to laser fluence. This significant effect of laser fluence on the LII decay time may be related to fragmentation or shape changes of the soot particles under intense laser heating.

(3) The LII signal was found to decay faster in regions where the mean soot particle diameter is smaller. To avoid the interference of elastic scattering and minimize particle-size effects, detection should be implemented immediately after the laser pulse, and the sampling (gate) time should be short (less than 50 ns).

(4) The technique has been used to obtain 2-D images of the soot volume fraction field in turbulent diffusion flames and a free-falling droplet flame, demonstrating that this technique can provide quantitative, instantaneous, and high spatially resolved measurements of soot volume fraction.

This material is based on work supported by the U.S. Office of Naval Research under grant N00014-93-0185, with Gabriel D. Roy as contract monitor, and the U.S. Air Force Office of Scientific Research under grant F49620-92-J-0161, with Julian Tishkoff as contract monitor, and is gratefully acknowledged. The authors also express their gratitude to B. Quay and M. Moser of Penn State for many useful discussions and technical assistance.

References

1. B. Quay, T.-W. Lee, T. Ni, and R. J. Santoro, "Spatially-resolved measurements of soot volume fraction using laser-induced incandescence," Combust. Flame **97,** 384–392 (1994).
2. T. Ni, S. B. Gupta, and R. J. Santoro, "Suppression of soot formation in ethene laminar diffusion flames by chemical additives," in *Twenty-Fifth Symposium (International) on Combustion* (The Combustion Institute, Pittsburgh, Pa., 1994), pp. 585–592.
3. N. P. Tait and D. A. Greenhalgh, "2D soot field measurements by laser induced incandescence," in the *Proceedings of the Optical Methods and Data Processing In Heat Transfer and Fluid Flow Conference* (Institution of Mechanical Engineers, London, 1992), pp. 185–193.
4. J. E. Dec, A. O. zur Loye and D. L. Siebers, "Soot distribution in a D.I. diesel engine using 2-D laser-induced incandescence imaging," Vol. SAE-910224 of the SAE Technical Papers Series (Society of Automotive Engineers, Warrendale, Pa., 1991).
5. J. E. Dec, "Soot distribution in a D. I. diesel engine using 2-D imaging of laser-induced incandescence, elastic scattering, and flame luminosity," Vol. SAE-920115 of the SAE Technical Papers Series (Society of Automotive Engineers, Warrendale, Pa., 1992).
6. L. A. Melton, "Soot diagnostics based on laser heating," Appl. Opt. **23,** 2201–2208 (1984).
7. P.-E. Bengtsson and M. Aldén, "Soot visualization strategies using laser techniques: laser-induced fluorescence in C_2 from laser-vaporized soot, and laser-induced soot incandescence," Appl. Phys. B **60,** 51–59 (1995).
8. C. R. Shaddix. J. E. Harrington, and K. C. Smyth, "Quantitative measurements of enhanced soot production in a flickering methane/air diffusion flame," Combust. Flame **99,** 723–732 (1994).
9. R. J. Santoro, H. G. Semerjian, and R. A. Dobbins, "Soot particle measurements in diffusion flames," Combust. Flame **51,** 203–218 (1983).
10. R. J. Santoro, T. T. Yeh, J. J. Horvath, and H. G. Semerjian, "The transport and growth of soot particles in laminar diffusion flames," Combust. Sci. Technol. **53,** 89–115 (1987).
11. A. C. Eckbreth, "Effects of laser-modulated particulate incandescence on Raman scattering diagnostics," J. Appl. Phys. **48,** 4473–4479 (1977).
12. C. J. Dasch, "Continuous-wave probe laser vaporization of small soot particles in a flame," Appl. Opt. **23,** 2209–2215 (1984).
13. R. L. Vander Wal and K. J. Weiland, "Laser-induced incandescence: development and characterization towards a measurement of soot volume fraction," Appl. Phys. B **59,** 445–452 (1994).
14. B. F. Magnussen, "An investigation into the behavior of soot in a turbulent free jet C_2H_2-flame," in the *Proceedings of the Fifteenth Symposium (International) on Combustion* (The Combustion Institute, Pittsburgh, Pa., 1975), pp. 1415–1425.
15. J. P. Gore and G. M. Faeth, "Structure and spectral radiation properties of turbulent acetylene/air diffusion flames," J. Heat Transfer **110,** 173–181 (1988).
16. R. C. Miake-Lye and S. J. Toner, "Laser soot-scattering imaging of a large buoyant diffusion flame," Combust. Flame **67,** 9–26 (1987).
17. J. H. Kent and S. J. Bastin, "Parametric effects on sooting in turbulent acetylene diffusion flames," Combust. Flame **56,** 29–42 (1984).